CROSSED MOLECULAR BEAM STUDIES OF SENSITIZED FLUORESCENCE

By

EUEL RAY CUTSHALL

A DISSERTATION PRESENTED TO THE GRADUATE COUNCIL
OF THE UNIVERSITY OF FLORIDA
IN PARTIAL FULFILLMENT OF THE REQUIREMENTS
FOR THE DEGREE OF DOCTOR OF PHILOSOPHY

UNIVERSITY OF FLORIDA

1977

ACKNOWLEDGEMENTS

The author wishes to thank many people for their contributions to this study. Of course, the main person that is to be thanked is Professor E. E. Muschlitz, Jr., whose guiding hand helped in so many ways. Professor Muschlitz was always willing to sit down and discuss any questions or problems that arose.

Dr. A. N. Schweid is the person responsible for design and construction of the majority of the apparatus. Without his initial help these studies would have taken much longer.

A special thank you goes to the men who work in the Electronics Shop of the Chemistry Department. Mr. R. J. Dugan is responsible for the design of several circuits unique to this experiment. Mr. J. W. Miller, Mr. J. B. Chamblee and Mr. W. Y. Axson were invaluable in keeping the electronic instrumentation operative. Mr. Axson and Mr. Chamblee have even worked on their own time on occasion to repair electronic components. Without their help the data for this study could never have been gathered.

To truly express my thanks to my wife would be impossible. She has been my constant companion and friend throughout the years of graduate work, and for this I am so very grateful.

TABLE OF CONTENTS

Abstract of Dissertation Presented to the Graduate Council
of the University of Florida in Partial Fulfillment
of the Requirements for the Degree of Doctor of Philosophy

CROSSED MOLECULAR BEAM STUDIES
OF SENSITIZED FLUORESCENCE

By

Euel Ray Cutshall

June 1977

Chairman: E. E. Muschlitz, Jr.
Major Department: Chemistry

Measurements have been made of the vibrational branching ratio (v'=0)/(v'=1) in N_2^* ($C\ ^3\Pi_u$) formed in the following reaction:

$$Ar(^3P_{2,0}) + N_2(X^1\Sigma_g^+) \rightarrow Ar(^1S) + N_2(C\ ^3\Pi_u)$$

by observation of the fluorescence N_2 ($C \rightarrow B$). The measurements were made in the relative energy range 0.053 to 0.408 eV using crossed supersonic molecular beams. Measurements have also been made of the N_2 (C, v'=0) to (B, v''=0) band profile at relative energies of 0.074 eV, 0.089 eV and 0.161 eV. Rotational temperatures of 1090°K and 1280°K were calculated from the 0.089 eV and 0.161 eV profile, respectively.

The vibrational branching ratio measurements have been compared to a theoretical "Golden Rule" model. The agreement is good in the low energy region from 0.053 eV to 0.15 eV.

CHAPTER I
INTRODUCTION

A. Historical Perspective

The first evidence for molecular beam formation was observed in 1883 by Fleming.[1] Using an incandescent lamp, he discovered that there was a shadow of the filament on the inside surface of the lamp apparently due to copper vaporized from the filament supports. From this he concluded that the copper molecules shot off the filament supports in straight lines. This agreed with the kinetic theory prediction that molecules have straight trajectories in the absence of molecular collisions or applied fields.

In 1911 Dunoyer designed the first molecular beam apparatus.[2] He used a glass tube under vacuum divided into three separate chambers by collimating holes. Heated sodium in the source chamber formed a deposit on the wall of the third chamber. The shape of the deposit indicated that a molecular beam of sodium had been formed. In 1921 the famous Stern-Gerlach experiment was conducted.[3] In this experiment a beam of silver atoms was deflected in an inhomogeneous magnetic field. These results verified the existence of space quantization and electron spin. Also, the magnetic moment of the electron was calculated. This experiment showed that

molecular beams would be of great value in investigating physical phenomena previously inaccessible to experimental analysis.

By 1928 using source pressures much greater than were previously thought possible, Johnson obtained molecular beams of much greater intensity than previous beams.[4] The Knudsen number, the ratio of the mean free path to the orifice diameter, of Johnson's source was 0.001 and thus was well into the range of continuum flow and could be classified as a nozzle beam source.

Johnson's work was for the most part ignored until Kantrowitz and Grey revived the idea in 1951.[5] They proposed the use of a molecular beam source in which continuum flow dominated rather than free molecular flow as in the previous effusive type sources. In this type of source they stated that beam intensities several orders of magnitude greater than effusive sources might be attained. Also, they believed that in this type of source the velocity distribution would be much narrower than in the effusive source.

These ideas were quickly implemented by Kistiakowsky and Slichter.[6] Although they showed that higher beam intensities were possible, their apparatus lacked sufficient pumping speed to show how effective the new design was.

In 1954 Becker and Bier designed a similar apparatus with a higher pumping speed and obtained beam intensities approaching that predicted by Kantrowitz and Grey.[7] Two years later Becker and Henkes measured the velocity distribution of argon atoms from a nozzle beam source.[8] They found a narrowed

velocity distribution as was again predicted by Kantrowitz and Grey. In these experiments the advantages of nozzle beam sources over effusive sources were conclusively demonstrated.

B. Use of Nozzle Beams to Study Electronic Energy Transfer Processes

The transfer of electronic energy from one species to another plays a very important role in many phenomena. These processes occur, for example, in electrical discharges, combustion, high temperature shocks, secondary processes in radiation chemistry, upper atmosphere reactions and laser action, with the main emphasis today in this last area.[9] The operation of laser systems such as Ar-O_2 and He-Ne is due to electronic energy transfer which serves as the excitation mechanism.[10]

The molecular beam technique has recently proved to be a valuable tool in the study of electronic energy transfer processes. Using molecular beams, it is possible to measure, for certain excited states, the velocity distribution of reaction cross sections, the angular distribution of reaction products, and the internal and kinetic energy distributions of these products.[9,11-14] In addition, by using molecular beams from nozzle sources, greater intensities with wider ranges of relative velocities and narrower velocity distributions are possible.

C. Purpose and Scope of Present Study

In this investigation a crossed nozzle beam study of electronic energy transfer has been conducted for the following reaction:

$$Ar(^3P_{2,0}) + N_2(X^1\Sigma_g^+) \rightarrow Ar(^1S) + N_2(C^3\Pi_u)$$

in the relative energy range 0.053 - 0.408 eV by observing the light emitted in the transition from the N_2 C state to the B state. This process is known as sensitized fluorescence.[15]

It has been shown previously by Fishburne that the metastable argon states ^3P_o (11.72 eV) and $^3P_2$ (11.54 eV) upon collision with ground state N_2 molecules give $N_2(C^3\Pi_u)$ which subsequently fluoresce to yield $N_2(B^3\Pi_q)$.[16] The lifetime of the N_2 C state has been reported as 28 nsec; therefore, all of the sensitized fluorescence occurs at the intersection of the two beams.[17]

The purpose of this study is to repeat the measurements made by Schweid on product vibrational energy distributions in this system using a much greater metastable intensity and over a wider relative energy range, and to extend the work to include measurements of rotational energy distributions.[9]

CHAPTER II
DESCRIPTION OF APPARATUS

A. Introduction

The molecular beam apparatus used in this study is shown in Figure 1. The sections which have not been modified since the work of Sanders are described in more detail in that reference.[18] The modifications include the following: A monochromator has been added to the optical system, the low voltage D. C. discharge cell for the production of metastable atoms has been replaced by an electron gun and the effusive source and velocity selector have been replaced by a supersonic nozzle beam.

A schematic drawing of the apparatus is shown in Figure 2. It consists of three differentially pumped vacuum chambers, gas inlet manifolds for the two nozzle beams and the electronic instrumentation required for time-of-flight studies and for measuring low level fluorescent light intensities.

The target beam is a supersonic nozzle beam of N_2 which is formed by maintaining a high pressure behind a very small circular orifice in the nozzle cap. The beam is collimated by a skimmer mounted on the wall of the target gas chamber and also by a collimating hole located in the main chamber. A mechanical chopper modulates the target beam which then inter-

Figure 1

Main Vacuum Chamber

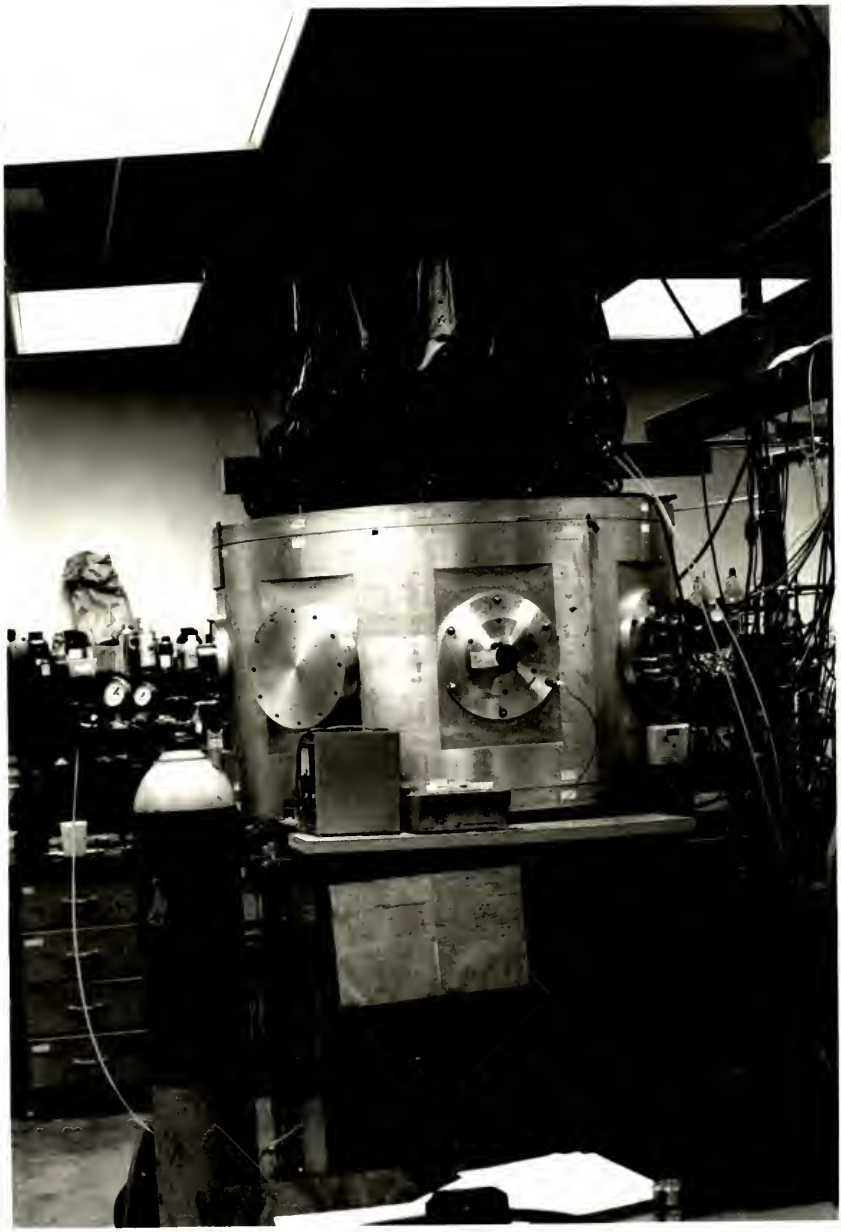

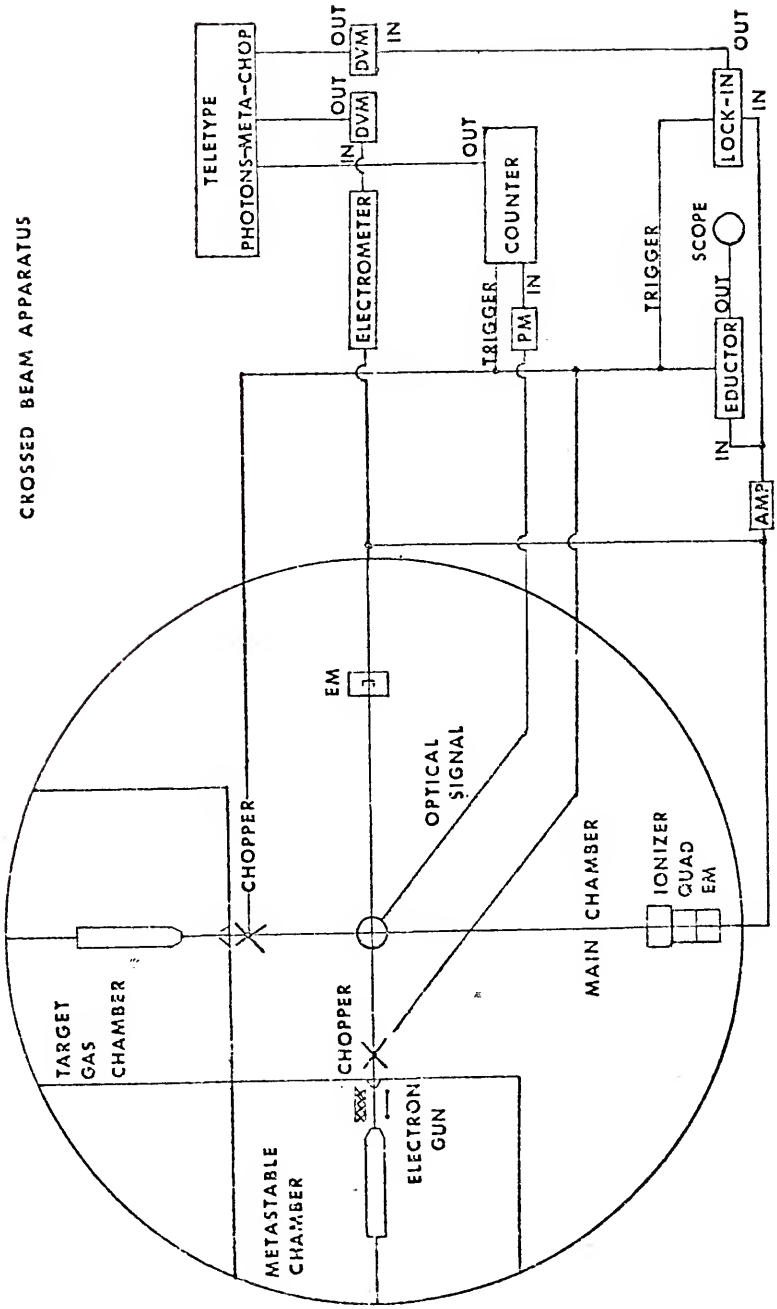

Figure 2. Crossed Beam Apparatus

sects the metastable beam at right angles. Finally, the beam enters a quadrupole mass spectrometer and is velocity analyzed by determining its flight time.

The metastable beam is also a supersonic nozzle beam. Metastable argon is produced by an electron gun which sets up a glow discharge between the nozzle and skimmer. After exiting the metastable chamber, the metastable atoms pass between a pair of deflector plates which sweep out any ions or electrons. The beam then passes through a collimating hole in the main chamber and a mechanical chopper which is used only during time-of-flight measurements. After intersecting the target beam, the metastable beam may be intercepted by a movable beam flag or allowed to pass on to the metastable atom detector, a magnetic electron multiplier.

Fluorescent light produced in the interaction zone, the region where the metastable and target beams collide, is detected by photon counting techniques. After being collected and focused, the photons pass through a monochromator which only transmits those photons in a selected wavelength range. Finally, the photons reach the cathode of a photomultiplier; the pulses from which are amplified and then counted by a dual channel photon counter. Signal averaging is accomplished by synchronizing the counter gates with the target beam modulation frequency.

The various components of the apparatus are described in detail in the following sections.

B. Gas Inlet Manifolds and Vacuum Chambers

A schematic drawing of the gas inlet manifold used for delivering gas to the nozzle in the metastable chamber is shown in Figure 3. Prior to its use in an experiment the metastable gas inlet manifold is evacuated by a roughing pump to a pressure of 50 microns or lower as read on a Pirani gauge.[19,20]

The argon used is manufactured by Airco Industrial Gases of Murray Hill, New Jersey, and is rated at better than 99.995 % purity. After leaving the storage cylinder, the argon passes through valve 1, the argon regulator shutoff valve, and valve 2, a solenoid valve used to mechanically stop the argon flow into the metastable chamber in case of power failure.[21] The argon then passes through a coiled copper tubing trap cooled to dry ice - acetone temperature. This trap removes any condensable impurities from the argon which might contaminate the filament or attenuate the metastable beam. After passing through shutoff valve 4, the argon goes through a leak valve which serves both to regulate the amount of gas flowing through the nozzle and to reduce the pressure of the gas coming from the argon tank.[22] The pressure behind the orifice in the nozzle cap is then read off an absolute pressure gauge.[23] Finally, the argon passes through shutoff valve 7 and a 7 micron mesh filter before going into the nozzle.[24] The filter removes any small particles which might clog the small nozzle opening. During normal operation valves 3, 5 and 6, a pump-out valve, are closed.

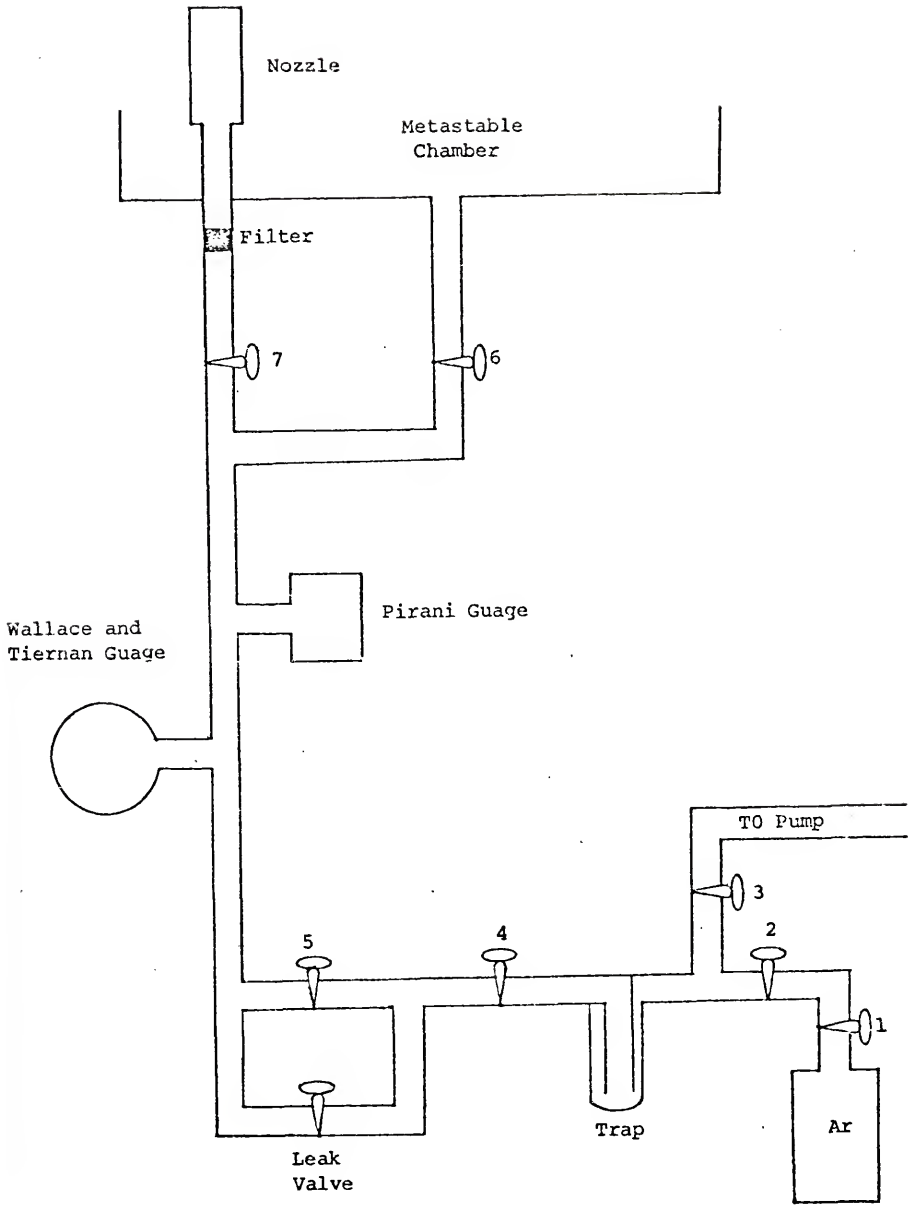

Figure 3. Metastable Chamber Gas Inlet Manifold

A schematic drawing of the target gas manifold is shown in Figure 4. Features of this manifold assembly such as the filter, the leak valves and the gas cylinders are identical to that of the metastable gas manifold. Again, the initial pumpout procedure involves evacuating the gas lines by a roughing pump to a pressure of 50 microns or lower as read on a thermocouple gauge.[25,26a] All of the numbered valves except 2 and 5, the solenoid valves designed to stop the gas flows in case of power failure, are shutoff valves. During normal operation with a seeded beam valves 1, 2, 5, 6, 7, 8 and 10 are open. The leak valves are adjusted to give the desired backing pressure, as read on an absolute pressure gauge, behind the nozzle orifice and also to give the desired flow rates of seeded (N_2) and seeding (He or Ar) gases.[23] The flow rates are monitored with mass flowmeters located just before each leak valve.[27] Seeding conditions from day to day can be reproduced by reproducing mass flowmeter readings.

All three differentially pumped chambers are evacuated by oil diffusion pumps backed by roughing pumps. Six-inch oil diffusion pumps with Mexican hat cold caps are used in both the target gas and metastable chambers.[28a] Additionally, there is a water-cooled baffle between the diffusion pump and the metastable chamber to prevent diffusion pump oil from getting inside and contaminating the filament used for metastable atom production.[28b] The voltage to both six-inch diffusion pump heaters can be varied between 0 and 240 volts

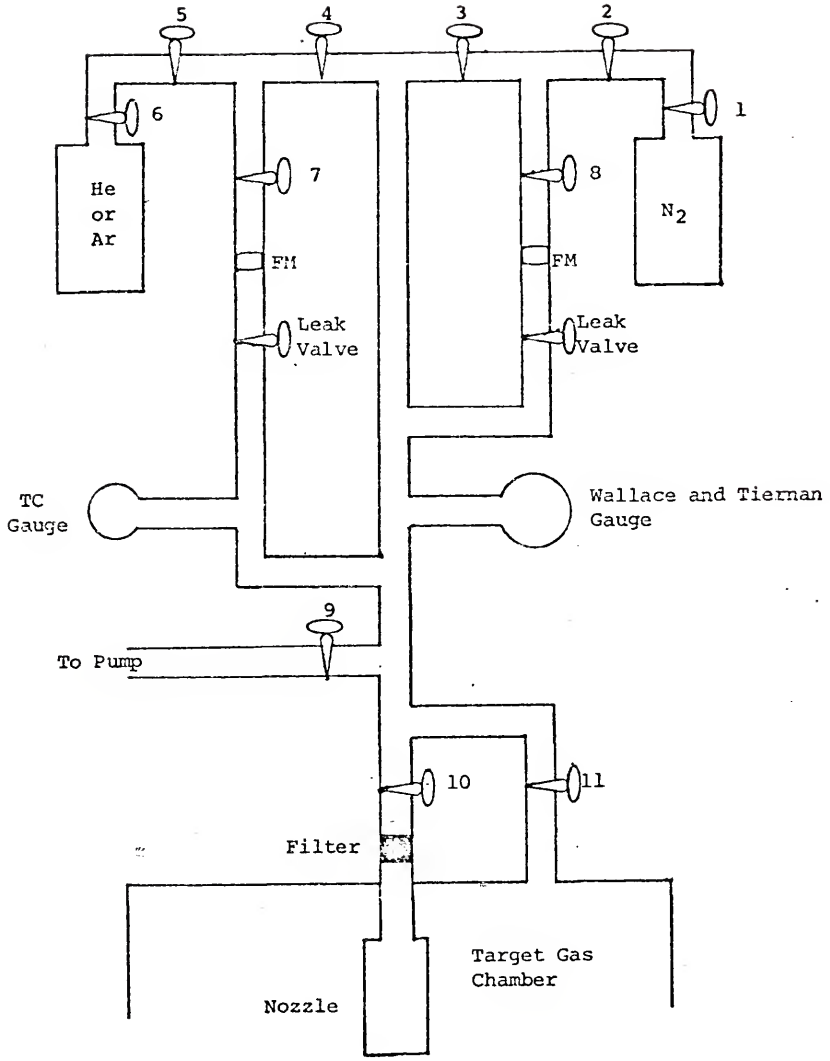

Figure 4. Target Chamber Gas Inlet Manifold

using adjustable A. C. autotransformers.[29] These were installed to prolong heater lifetime by reducing the A. C. voltage input and thereby the heater current. It was found experimentally that the heater voltage could be reduced to 200 volts without any loss of pumping speed by the diffusion pumps. The main chamber has a ten-inch oil diffusion pump and a freon-refrigerated baffle.[26b,30] Because of the high pumping speed requirement for nozzle beams, sizable roughing pumps are used on all three chambers.[31] The foreline pressures of all three chambers are monitored by thermocouple gauges, and the chamber pressures are monitored by ionization gauges.[32,33] Typical static chamber pressures are given below:

Metastable chamber: 1×10^{-6} torr

Target gas chamber: 1×10^{-7} torr

Main chamber: 1×10^{-6} torr

C. Metastable Beam Production and Analysis

In this study metastable argon atoms are produced in a glow discharge which is initiated and sustained by an electron gun between the nozzle and the skimmer. This configuration is shown in Figure 5.

The nozzle used here is made in two pieces, the body and the cap. The body is a brass cylinder 3 inches long and 0.625 inches in diameter with a 0.0625 inch hole drilled through its center to accommodate the argon flow. Also, the

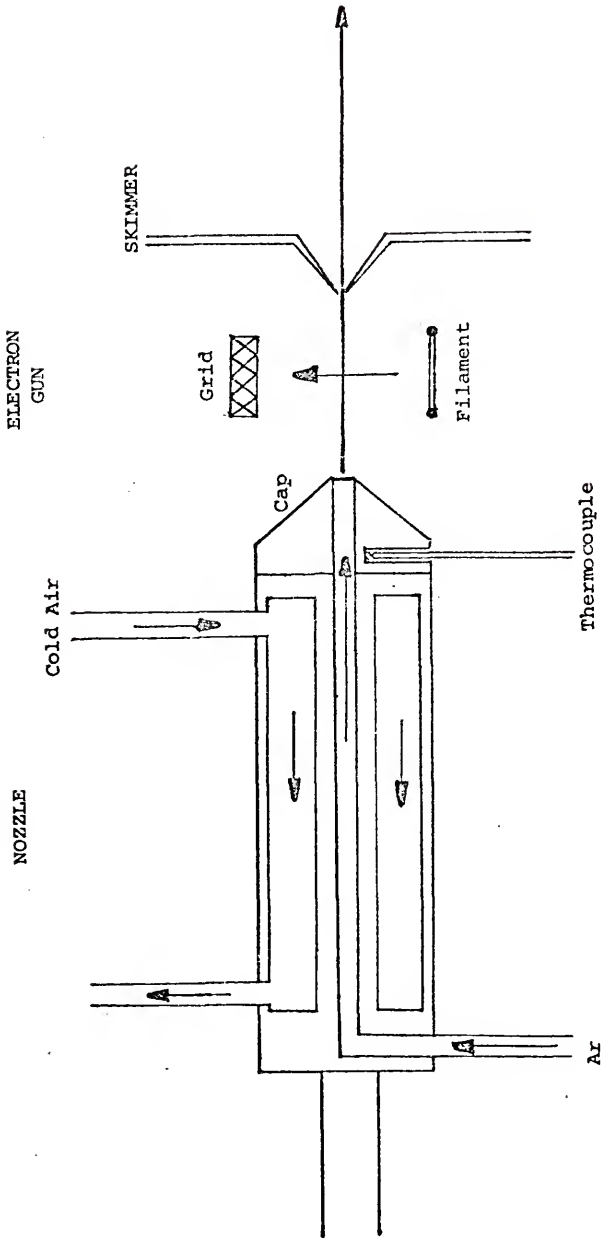

Figure 5. Metastable Beam Nozzle

body is made in such a way that there is a cylindrical cooling channel between the outside wall and the inside flow tube. In certain experiments when it is necessary to cool the nozzle, cold air is forced through the cooling channel. The air is cooled by passage through a coil of copper tubing immersed in a dry ice - acetone bath. The nozzle cap is a truncated cone made of Inconel. Inserted in the end of the cap is a 3 mm O. D. molybdenum wafer with a 0.002 inch diameter hole in its center.[34] An Iron-Constantan thermocouple used for measuring nozzle temperature is inserted into a small hole drilled in the side of the nozzle cap. The thermocouple output is fed to a temperature controller which gives a direct readout of nozzle temperature.[35a]

The skimmer, a hollow brass cone with a 0.040 inch diameter opening in the tip, is screw mounted to the metastable chamber wall. It removes unused gas from the axis of the beam and also defines the beam path.

A stainless steel rod attached to the rear of the nozzle is coupled through the vacuum chamber wall to a micrometer screw mechanism on the outside of the apparatus which gives a direct reading of the nozzle cap to skimmer distance. The nozzle is connected to the argon inlet line by a flexible stainless steel tube. Likewise, flexible stainless steel tubes are used to connect the inlet and outlet of the cooling channel to the inlet and outlet for the cold air flow. By using this type of tubing as connectors, the nozzle - skimmer distance can be adjusted. It was determined experimentally

that a nozzle - skimmer distance of 0.420 inches gave the greatest metastable intensity as measured by the magnetic electron multiplier.

The electron gun used in these experiments for metastable atom production is shown in more detail in Figure 6. It is a very simple design consisting basically of only a heated filament and a grid. The filament is heated by a low voltage, high current power supply.[36] The electrons "boiled off" are repelled from the filament due to its -10 V potential, supplied by a separate power supply, and attracted toward the grid due to its +65 V potential, supplied by still another power supply.[37,38] The path of the electrons crosses the path of the argon beam at an angle of 90°. These electrons initiate and sustain a glow discharge directly across the path of the argon. Metastable argon atoms are formed in the glow discharge and exit the metastable chamber through the skimmer.

The filament and its supports are spot welded together. Nickel tabs bent at a 90° angle are spot welded directly to high current headers in the filament block assemply. The filament, a piece of iridium ribbon about one inch long, is then sandwiched between and spot welded to the nickel tabs. The shield, a small rectangular piece of nickel sheet, protects the high current headers from the heat generated by the filament. After the filament assembly is spot welded together, the filament is cataphoretically coated with thoria.

The grid consists of a 0.050 inch nickel wire frame to

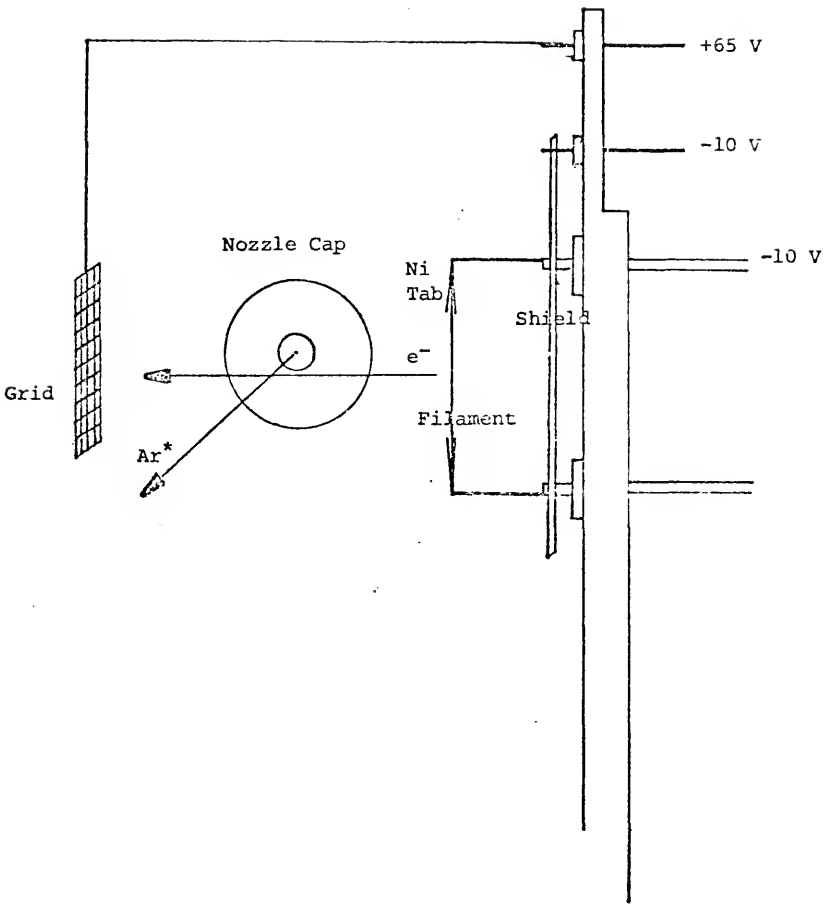

Figure 6. Electron Gun

which 0.003 inch nickel wires have been spot welded.

After the metastable argon beam leaves the metastable chamber through the skimmer, it passes directly between a pair of deflector plates, one of which is at ground potential and the other at +300 V. This effectively removes any ions or electrons from the metastable argon beam. The beam is further defined by passing through a 0.079 inch diameter collimating hole in the main chamber.

The beam then arrives at a mechanical chopper assembly. During the photon counting portion of an experiment the chopper is open and not in use. It is rotated at a speed of 50 hertz and is used only when a time-of-flight velocity analysis is carried out on the beam. A schematic drawing of the chopper is given in Figure 7. It is similar to the target gas chopper; and a detailed description of the circuitry, instrumentation and procedure used for measuring the velocity distribution is given in the next chapter. The two analyses are identical except for the fact that the metastable atom detector is a magnetic electron multiplier, while the target gas detector is a quadrupole mass spectrometer.

Each revolution of the chopper allows two sets of two beam pulses to pass, one short set and one long set. Also, simultaneously with each beam pulse that is passed an electrical signal is produced by a photocell located 180° away from the beam position. The short beam pulses, produced by the narrow 0.010 inch slot, are used in the time-of-flight analysis of the beam. The long beam pulses (5.0 msec wide) are not used.

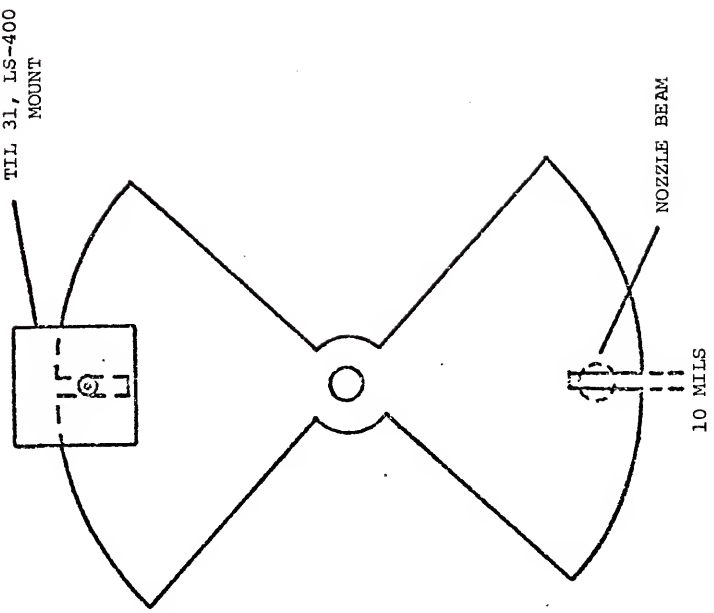

Figure 7. Metastable and Target Beam Chopper

After passing through the intersection zone, the metastable beam arrives at a magnetic electron multiplier shown in Figure 8.[39] This electron multiplier serves two purposes: First, when the chopper is rotating, a velocity analysis can be carried out on the metastable beam; and second, when the chopper is open and not rotating during the photon counting portion of an experiment, it allows the metastable beam intensity to be monitored. The output current from the electron multiplier is measured by an electrometer using a 1 megohm input resistor.[40] This current is proportional to the metastable atom flux and is monitored continuously on a digital voltmeter and chart recorder during an experiment.[41,42]

D. Target Beam Production and Analysis

A schematic drawing of the components which form the target beam nozzle is shown in Figure 9. The nozzle is made entirely of Inconel and is screw mounted together. The center of the nozzle has a 0.002 inch hole drilled in it which serves as the nozzle opening. As in the metastable chamber, the rear end of the nozzle has an Inconel rod attached to it which is coupled through the chamber wall to a micrometer dial outside the apparatus. The distance read on the micrometer dial is the distance between the nozzle cap and the tip of the skimmer. The skimmer used here is identical to the one used in the metastable chamber. The oven is connected to the target gas inlet by a flexible copper tube. This allows the

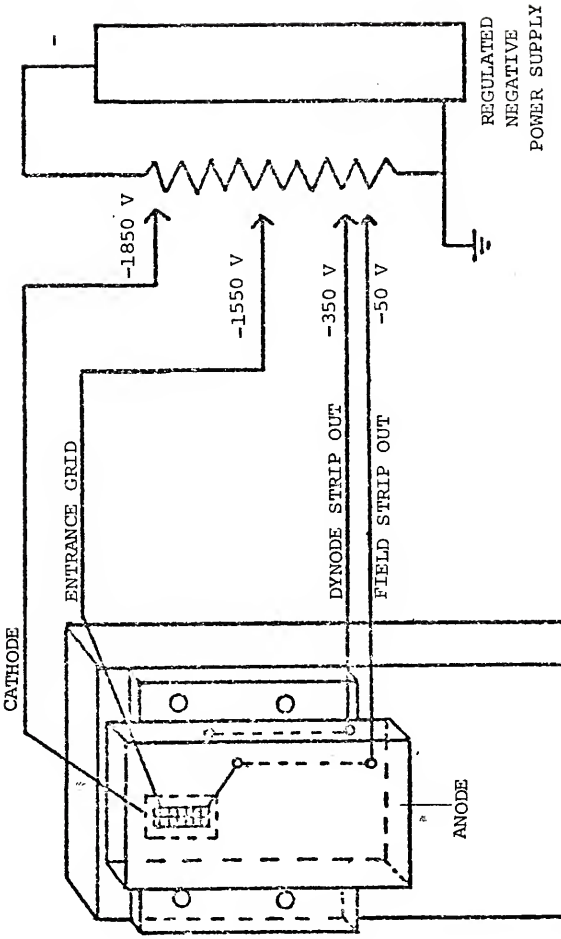

Figure 8. Magnetic Electron Multiplier

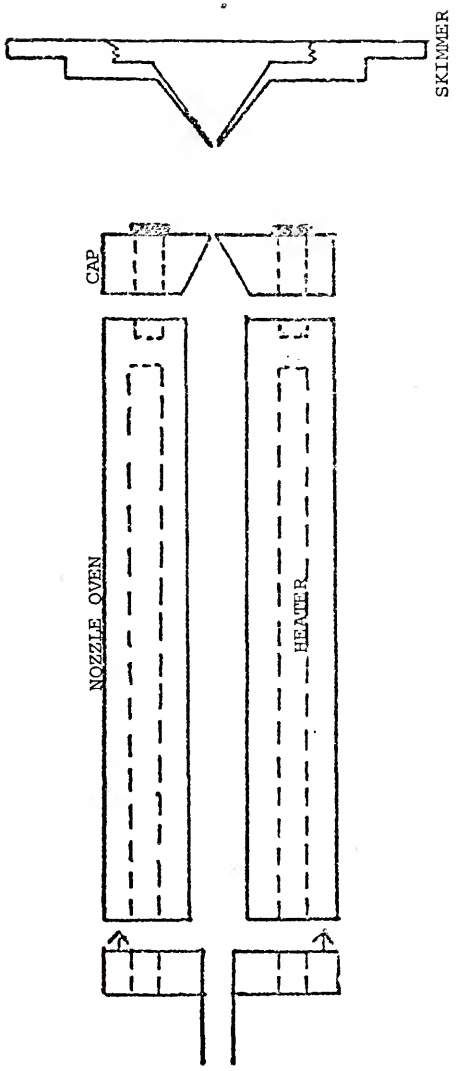

Figure 9. Target Beam Nozzle

nozzle - skimmer distance to be changed for optimization of target beam intensity, and it was determined experimentally that a nozzle - skimmer distance of 0.400 inches gave the greatest fluorescent light intensity.

The heater is a long strand of tantalum wire strung back and forth from one end to the other of the oven through three alumina insulators. The alumina insulators are mounted in the oven 120° away from one another. The power supply used to heat the tantalum wire is an A. C. autotransformer coupled to a high current filament transformer. With this supply the nozzle can easily be heated to 400°C. The temperature is measured by a Chromel-Alumel thermocouple and read directly from a temperature controller.[35b]

By heating, the velocity of the target beam can be greatly increased from its room temperature value. The relationship between beam energy and oven temperature in the limit of complete expansion is given below:[43]

$$E_z = C_p T_o \qquad (1)$$

Here E_z is the translational energy directed along the beam axis, C_p is the specific heat of the beam gas at constant pressure, and T_o is the oven temperature.

The velocity of the target gas can also be increased by seeding; that is, mixing the target gas with a lighter one. The light gas, He, accelerates the heavy N_2 gas molecules to higher velocities.[44] For high gas densities the velocity of both components of the gas will be the same; however, the two components have different masses and therefore different

translational energies.[43] The energy of a molecule of component i is given by

$$E_i = \frac{M_i}{\bar{M}} \bar{C}_p T_o \qquad (2)$$

where M_i is the molecular weight of component i, $\bar{M}$ is the average molecular weight and $\bar{C}_p$ is the average molar heat capacity. It should be noted that the seeding technique can also be used with a gas heavier than the target gas, i.e., reverse seeding. Reverse seeding using argon reduces the translational energy of the target gas.

The following expression has been derived by Anderson and Fenn for relative beam density as a function of relative flight time:[45]

$$\frac{S}{S_{max}} = \frac{1}{\tau^4} \exp\{-\tfrac{1}{2} M_s^2 [(\frac{b}{\tau} - 1)^2 - (b - 1)^2]\} \qquad (3)$$

$$b = \tfrac{1}{2}[1 + (1 + \frac{16}{\gamma M_s^2})^{\frac{1}{2}}]$$

where S/S_{max} is the ratio of the beam density at a particular flight time to the maximum beam density, τ is the ratio of the time-of-flight to the time-of-flight for which S is a maximum, γ is the specific heat ratio C_p/C_v, and M_s is the Mach number at the skimmer entrance. The Mach number is defined as the ratio of the stream velocity u along the beam axis to the local speed of sound in the gas: $M_s = u/(\gamma kT/m)^{\frac{1}{2}}$. Using equation (3) the Mach number which best characterizes the nozzle beam may be estimated by comparison with the experimentally determined velocity distribution. In previous work it was found

that a Mach number of 10 best described the nozzle velocity distribution.[18] The same result should hold true for the metastable nozzle because of its similar design.

The target beam enters the main chamber through the skimmer and is further defined by a 0.079 inch diameter collimating hole. The beam then encounters the same type of chopper assembly (Figure 7) as the one used with the metastable beam. The chopper is powered by a synchronous hysteresis motor which is driven by an amplified oscillator signal.[46,47] During an experiment the chopper rotates at a speed of 50 hertz and therefore modulates the target beam at a frequency of 100 hertz. The beam modulation permits both a velocity analysis to be carried out on the target beam and signal averaging to be conducted with the photon flux.

As with the metastable beam each revolution of the chopper produces 2 long and 2 short pulses. The photocell produces an accompanying electrical pulse for each beam pulse. The short beam pulses travel across the main chamber to the target beam detector where they are velocity analyzed. The long beam pulses contain the molecules that produce the photon signal. After traveling through the interaction zone, the target beam molecules reach the target beam detector, a quadrupole mass spectrometer, which is shown schematically in Figure 10.[48a] A 0.070 inch slit further collimates the beam before it enters the ionizer. Ionization of the beam is accomplished by electron impact. The ions are then swept into the quadrupole and mass analyzed to separate the target

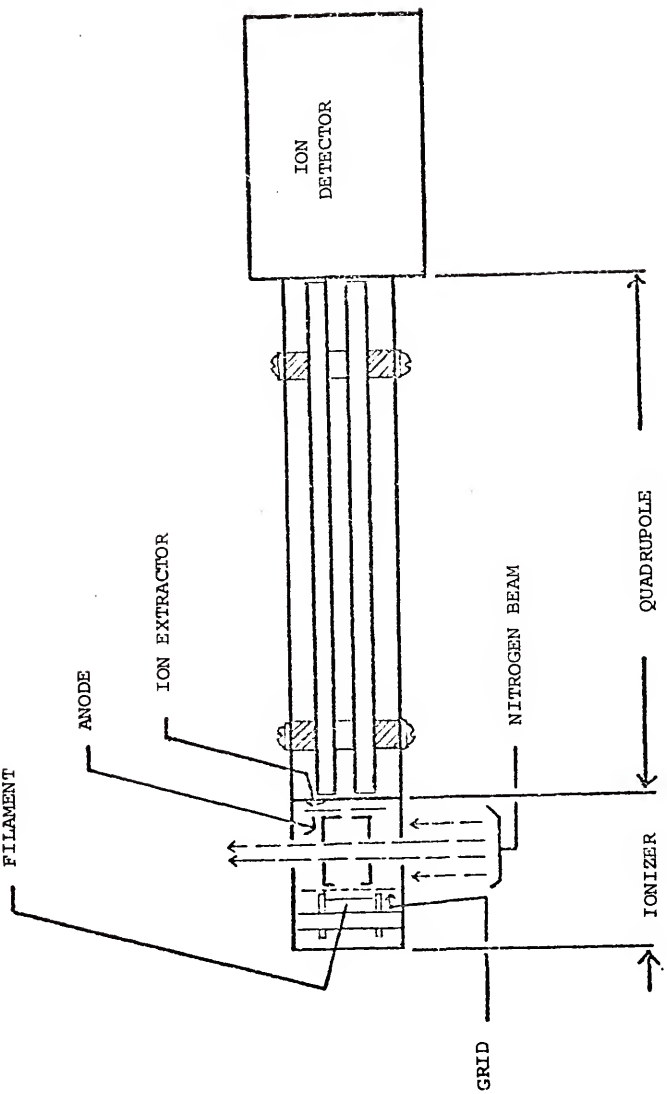

Figure 10. Quadrupole Mass Spectrometer

and seeding gases. The quadrupole is set at mass 28 (N_2^+) for these studies. An electron multiplier provides the current output signal from the quadrupole.[48b] This current signal is converted to a voltage signal by the beam pulse amplifier, a specially designed 2 stage amplifier.[49]

The pulses from the photocell provide both a trigger signal for the photon counter and a zero-time reference signal for the beam velocity analysis. The alternating long and short photocell pulses are first shaped into square waves by a Schmitt trigger circuit and then separated into separate trains of long and short pulses by a pulse separator.[50,51] The time relationship between the photocell pulses and the beam pulses is shown in Figure 11.

The output of the first stage of the beam pulse amplifier is fed into a lock-in amplifier whose reference signal is the train of long optical pulses.[52a] The output of the lock-in amplifier is read directly from a digital voltmeter and is proportional to the target beam intensity.[53] The output of the second stage of the beam pulse amplifier is fed into a waveform eductor which is triggered by the short optical signal, the zero-time signal.[52b] The eductor scans and signal averages an adjustable time segment of the beam signal, that segment which corresponds to the short beam pulse. Both the short optical signal and the waveform eductor output are displayed on a dual beam oscilloscope.[54a] The time between the rise of the short optical signal and the maximum of the time-of-flight peak from the eductor gives the flight time

Figure 11. Pulse Timing Relationships

A. Output from pulse shaping circuit
B. Short pulses for triggering waveform eductor
C. Long pulses for triggering lock-in amplifier
D. Long pulses, delayed 200 μsec for triggering SSR
E. Output from I → V converter/amplifier
Δt = time-of-flight

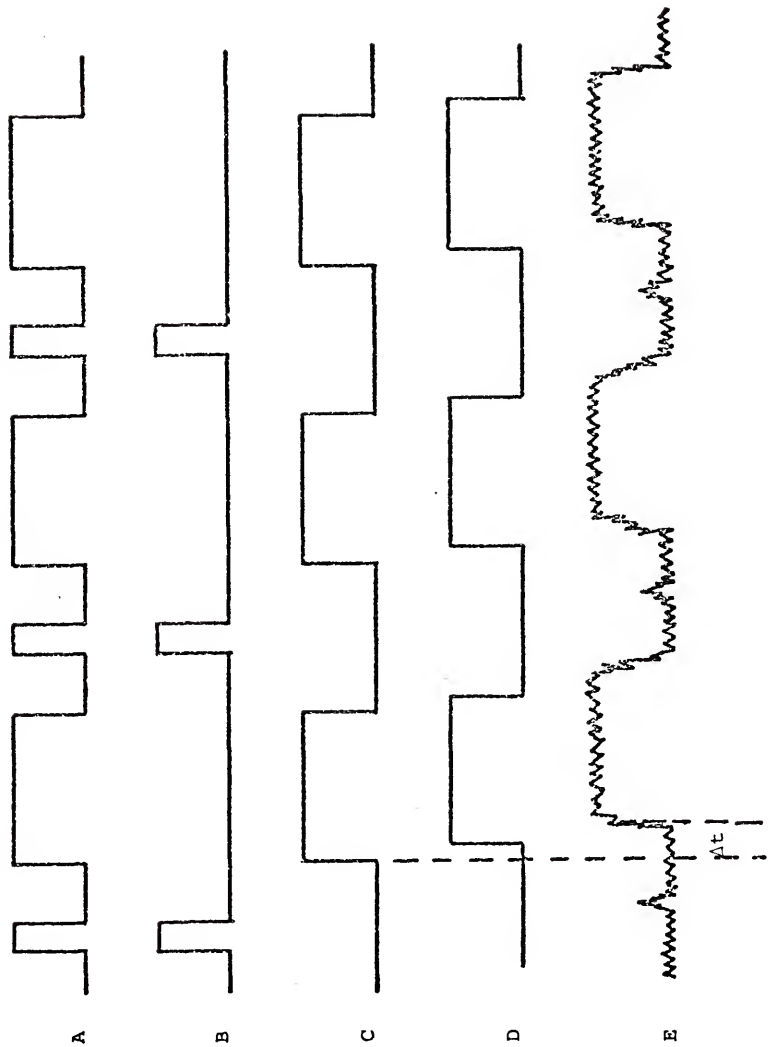
A
B
C
D
E
Δt

of the target beam. It was determined experimentally that each beam pulse was delayed 6 μsec in traveling through the beam pulse amplifier; therefore, 6 μsec was subtracted from each flight time measured before a velocity calculation was carried out.

The short optical signal may also be fed into a crystal clock timer which provides an output pulse at a known adjustable delay time after the rise of the short optical signal.[55] This timer pulse, which rises at a known preset time after zero-time, can then be fed into the oscilloscope instead of the short optical pulse. The time between the timer pulse and the maximum of the time-of-flight peak can then be measured on the scope on a faster time scale. This yields a more accurate flight time determination.

E. Photon Collection and Detection

The fluorescent light emitted in the interaction zone is collected and focused by a concave mirror - lens system onto the entrance slit of a monochromator. Light exiting the monochromator is focused by another lens onto the cathode of a photomultiplier. This arrangement is shown in Figure 12.

In order to double light collection efficiency a concave mirror is located below the plane of the molecular beams at a distance equal to its radius of curvature (20.0 mm).[56a] A biconvex lens, lens 1, is located above the plane of the molecular beams at a distance equal to its focal length (25

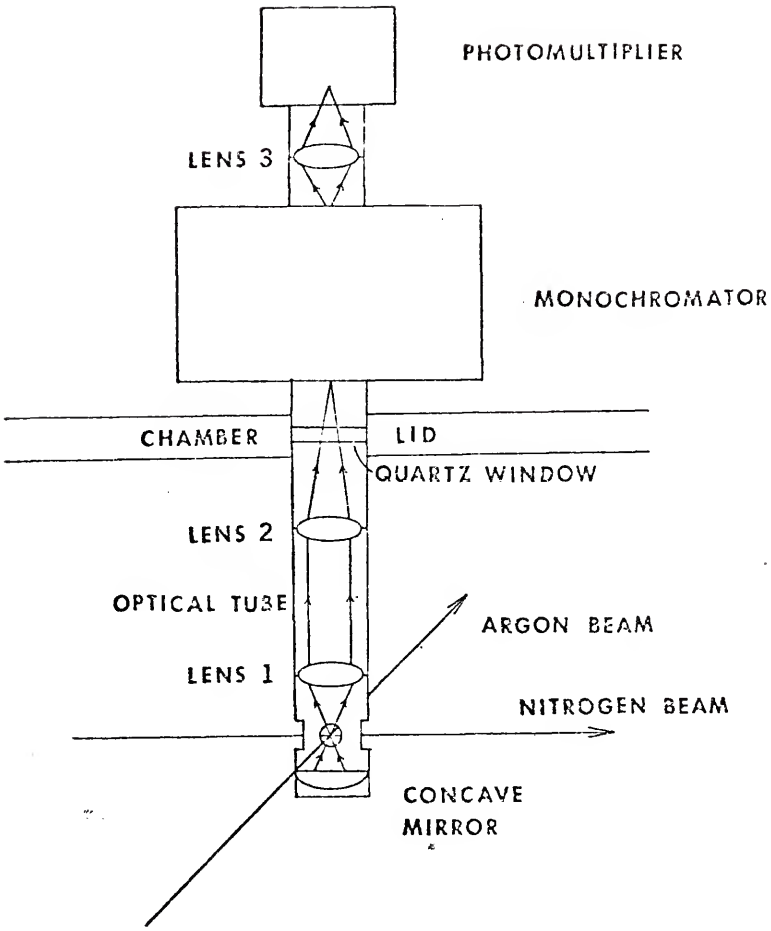

Figure 12. Photon Collection and Analysis

mm).[56b] Photons collected by this lens are directed upward with parallel paths. The photons are focused by another biconvex lens, lens 2, through a quartz window onto the entrance slit of a monochromator which selects the desired wavelength of light to be studied.[56c,57] The concave mirror and lenses 1 and 2 are mounted inside an aluminum tube (3 inches in diameter) which is fastened to the lid of the main chamber.

The monochromator utilizes a 1200 groove/mm grating with a 5000 Å blaze. The entrance and exit slits are removable and come in a variety of 5 different sizes corresponding to bandpasses of 10, 20, 50, 100 and 200 Å. The wavelength range of the monochromator is 1750 to 10000 Å with wavelength readings accurate to 10 Å.

Light leaving the exit slit of the monochromator strikes the cathode of a photomultiplier.[58] The monochromator and photomultiplier are located under the black plastic covering on the lid of the main chamber in Figure 1. The photomultiplier is cooled to -25°C by a thermoelectric refrigerator to reduce the dark noise.[59] Under these conditions with a bias potential of 1250 V on the photomultiplier the dark noise is reduced to about 12 counts sec^{-1}.[60] When photon measurements are not being made, a manual shutter just below the photomultiplier can be closed sealing it off from incoming radiation.

The wavelength response of the photon detection system has been discussed previously by Sanders.[18]

Pulses from the photomultiplier provide input to a linear amplifier and are counted by a digital synchronous computer.[61]

This photon counter operates in the "chop" mode and stores counts in two different channels, A and B. A gating signal derived from the long optical pulses from the target beam chopper is used to determine which channel receives counts at any particular time. The long optical pulse is fed into a pulse generator operated in the pulse delay mode.[54b] The pulse generator produces a 5 msec square wave just exactly like the long optical pulse except that it is delayed by 200 μsec. This is more than sufficient time for the N_2 to travel from the chopper to the interaction zone, about 2.2 inches, and fluorescence to begin. The delayed pulse is used as the gating signal for the photon counter. The rise of this pulse opens channel A of the counter, and counts are fed into this channel for a time preset on the rear of the counter - 4 msec in these experiments. These counts correspond to fluorescent emission counts plus background counts, since during the 4 msec interval the 5 msec target beam pulse is in the interaction zone. Channel A is then closed, and the next 1 msec is dead time. The fall of the delayed pulse opens channel B, and for the same preset time, counts are stored in this channel. These counts correspond to background counts only, for channel B is opened 200 μsec after the target beam chopper closes, and all of the N_2 target beam pulse has already left the interaction zone. The only fluorescence that is taking place is that due to the N_2 background gas, and this is constant whether the N_2 pulse is present or absent. Channel B is then closed after the same preset time of 4 msec, and the next 1 msec is again dead time. This long dead time was

chosen because it makes timing errors (such as slight variations in the chopper frequency) insignificant. The cycle starts all over again with the rise of the next delayed pulse, and the process is repeated for the number of cycles preset on a front panel control. The difference between the number of counts in channels A and B is the number of counts due to fluorescent emission from beam molecules only.

F. Data Output

The outputs of the electrometer used to monitor the metastable beam intensity and the lock-in amplifier used in time-of-flight determinations are displayed on two digital voltmeters.[62a] Also, the outputs of the two mass flowmeters which give the flow rates of the target and seeding gases are displayed on digital voltmeters.[63] The contents of these four voltmeters are fed to a teletype through a special interface.[62b,64]

When the number of cycles preset on the photon counter has been reached, the contents of channels A and B, their sum and their difference is printed on the teletype. On the next line the values of the four voltmeters are printed. The whole process automatically starts again, unless the interface is in the manual mode. In this case data collection stops until manually restarted.

G. Cryopump Assembly

Preliminary experiments were conducted to determine what the background count rates were at the wavelengths to be studied in this work. In these experiments the target beam was not used; only the metastable argon beam passed through the interaction zone. The wavelengths corresponding to two vibrational bands in the $C \rightarrow B$ transition of N_2 were observed. These were the $v' = 0$ to $v'' = 0$ band the the $v' = 1$ to $v'' = 0$ band corresponding to wavelengths of 3346 Å and 3135 Å, respectively. In order to measure the intensity of the entire band, slits allowing a 100 Å bandpass were used in the monochromator. With no nitrogen flowing through the interaction zone, the normal background count rate of about 12 counts sec^{-1} should be observed if no other reactions were producing any fluorescent light at these wavelengths. At 3346 Å the background was measured to be the expected value of 12 counts sec^{-1}. However, at 3135 Å the background count rate was approximately 350 counts sec^{-1}, nearly 30 times higher than expected.

From this it was concluded that some other reaction producing fluorescent light at or near this wavelength must be occurring. Using the quadrupole mass spectrometer, it was observed that the only other gas in the main chamber besides argon was water vapor, mass 18, which adsorbs strongly to the chamber walls. Therefore, the metastable argon must be reacting with water vapor to produce the light.

The spectrum of the light radiation from a pulsed discharge in argon with a small water vapor impurity has been investigated by Bertschinger et al.[65] A long lived band spectrum around 3090 Å was found which could not be attributed to known transitions in argon or Ar_2. It was concluded that the following reactions were taking place:

$$Ar(^3P_2) + H_2O \rightarrow Ar + H + OH(A^2\Sigma^+)$$
$$OH(A^2\Sigma^+) \rightarrow OH(X^2\Pi) + h\nu(3090\ \text{Å})$$

Metastable argon transfers electronic energy to an H_2O molecule, dissociating it and forming an electronically excited OH radical. The OH radical decays radiatively to its ground state producing light around 3090 Å. This same process sees to be occurring in the interaction zone.

A background intensity this high would reduce the signal-to-noise ratio and give less accurate experimental data. To reduce the background intensity at this wavelength a cryopump was installed. It is shown in Figure 13. Basically, it is a sealed stainless steel can, 5 5/8 inches in diameter and 5 inches long. Four-inch copper fins were strapped around the body of the can to increase the cooled surface area. A sidearm going into the can is welded to a stainless steel flange on the outside of the apparatus. The can is filled with liquid nitrogen through the sidearm which also serves as a vent for gaseous nitrogen. The cryopump filled with liquid nitrogen effectively reduces the partial pressure of water vapor in the main chamber. The background counts at 3135 Å are reduced from 350 to 50 counts sec^{-1} which is an acceptable value for the experiments done in this work.

Figure 13. Cryopump Assembly

CHAPTER III
EXPERIMENTAL PROCEDURE

Prior to the start of any experiment the three vacuum chambers and both gas inlet manifolds are evacuated to pressures at least as low as those mentioned in Chapter II B. This can be done overnight. Also, all electronic equipment to be used in an experiment is turned on during the initial pumpdown and allowed to warm up overnight.

After pumpdown, the gas flows into both the metastable and target gas chambers can be started. The regulators on the gas cylinders to be used in the experiment are adjusted to a value of 20 PSIG.

The argon flow rate into the metastable chamber is adjusted using the leak valve shown in Figure 3 so that the metastable chamber pressure as read on the ionization gauge is in the range 4 - 6 x 10^{-4} torr. This pressure range gives a glow discharge with the greatest stability. Once started the argon flow takes about 4 hours to come to equilibrium.

After pumpdown, the target gas flow should also be started. For an unseeded beam, only N_2 is fed into the target gas manifold. For a seeded beam, N_2 and the seeding gas, either He or Ar, are used. Flow rates for the N_2 and seeding gas are adjusted individually using the leak valves shown in Figure 4 to values which give the appropriate gas mixture for the

desired N_2 velocity. It should be mentioned that at times these valves are very sensitive, and small changes in their settings can lead to large changes in the gas flow rates. Each time a valve setting is changed, the gas flows and therefore, the N_2 velocity may take up to 8 hours to equilibrate. In any event, an experiment should not be started for at least 8 hours after the gas flows have been set. A typical backing pressure behind either nozzle opening is about 20 PSIA.

During some experiments the target beam nozzle is heated. If so, the A. C. heater is turned on after the gas flows are started; and the temperature of the nozzle is allowed to come to equilibrium during the same 8 hour period as for the gas flow. The nozzle temperature desired is set by applying the appropriate potential difference across the heater terminals and is monitored by a thermocouple connected to a temperature controller. These voltage values were determined experimentally and are listed in Table 1. These values depend to some extent on the gas mixture used in the nozzle. The values listed in Table 1 are for pure N_2.

At the beginning of each experiment the cryopump is filled with liquid nitrogen, and the probe of the liquid nitrogen indicator is inserted into the cryopump.[66] This indicator is connected to a buzzer which is energized whenever the liquid nitrogen in the cryopump falls below a certain level. Usually, the cryopump has to be refilled every 3 hours.

With the argon flow equilibrated, the glow discharge is

Table 1

Heater Voltage Values
For Certain Target Nozzle Temperatures

Heater Voltage (V)	Nozzle Temperature (°C)
2	100
9	200
17	292
23	350
30	400

started by gradually increasing the current going through the filament in the electron gun. The filament current is slowly increased in 1 amp steps with a 2 minute waiting period between each increase. The filament is biased at -10 V (anode voltage) with respect to ground, and the grid at +65 V with respect to ground. However, it was found that the glow discharge started much more easily if the anode voltage were initially set at -50 V. After the glow discharge starts, the anode voltage is then reduced to the -10 V value. The filament current is increased to a value which gives an emission current of about 75 milliamps and a corresponding grid current of about 70 milliamps. These currents are monitored on analog type milliammeters.[67] The above current values were chosen because they gave very adequate metastable intensities which were much more stable than with higher emission current values.

The metastables are detected by a magnetic electron multiplier; the current output of which is measured by an electrometer and recorded on a chart recorder. The metastable intensity takes 3 - 4 hours after start up to settle down to a constant value. After the metastable intensity has stabilized, the photon counting part of the experiment can begin.

For the lower relative energy measurements between metastable argon and N_2 it was necessary to cool the metastable nozzle. This was accomplished by forcing cold air through a hollow cylindrical jacket surrounding the nozzle (see Figure 5). The air used for cooling contains water vapor which has to be trapped out prior to entering the copper cooling coil

which is immersed in a dry-ice - acetone bath. Otherwise, the cooling coil would soon become blocked by ice. The water vapor is condensed out before it enters the cooling coil by running the air through two glass traps in series which are also immersed in dry ice - acetone baths. From the cooling coil the air goes directly to the nozzle jacket and back out of the metastable chamber through a vent. The temperature to which the nozzle is cooled can be adjusted by changing the flow rate. The nozzle temperature is monitored using a thermocouple connected to a temperature controller. Although the controller was set up to read temperatures only in the range 0 - 200°C, by reversing the thermocouple input leads and recalibrating the instrument, temperatures to -100°C could be measured. It was found that the metastable nozzle could be cooled as low as -36°C. After the cool air flow is started, it takes about 2 hours for the nozzle temperature to come to equilibrium.

Just prior to the photon counting portion of the experiment time-of-flight measurements are carried out on the metastable argon and the N_2 beams as described in Chapter II C and II D. The shutter between the monochromator and the photomultiplier is then opened, and photon counting begins. Only 2 bands of C state to B state emission from N_2 were studied, the v' = 0 to v'' = 0 band and the v' = 1 to v'' = 0 band.

In one series of experiments slits allowing a 10 Å bandpass were placed in the monochromator, and band profile measurements were carried out on the (0 - 0) band at different

relative energies of N_2 and metastable argon. The wavelength range for the profile measurements was from 3310 Å to 3375 Å. Intensity limitations prevented a profile study of the (1 - 0) band.

In the other series of experiments conducted, slits allowing a 100 Å bandpass were used in the monochromator to measure total photon intensities from the (0 - 0) and (1 - 0) bands. In these experiments light from the entire band had to be collected. Therefore, the monochromator was not set at the band heads which are 3370 Å for the (0 - 0) band and 3158 Å for the (1 - 0) band; but rather at lower wavelengths in each band which were determined experimentally to give the largest photon signal.[68] The experimental wavelength settings are 3346 Å for the (0 - 0) band and 3135 Å for the (1 - 0) band. Data points were taken alternately in sets of 3 for each wavelength until at least 15 data points for each wavelength were obtained.

The photomultiplier shutter is then closed, and time-of-flight measurements are again taken for both beams. This is done as a check to make sure relative energy conditions of the two beams have not changed. No changes greater than 1% were ever noticed.

At the end of each experiment the remaining liquid nitrogen in the cryopump is blown out using compressed air, and the cryopump is evacuated overnight using a roughing pump to remove any water remaining inside.[25] If this were not done, water in the bottom of the cryopump would seep in between the

bottom and side of the stainless steel can and might crack the bottom weld of the cryopump when frozen by liquid nitrogen in the next experiment.

CHAPTER IV
BEAM CHARACTERIZATION EXPERIMENTS

A. Metastable Beam

The dimensions associated with the metastable argon beam are listed in Table 2.

A preliminary experiment was done in this study to determine the metastable atom intensity. In this experiment a Faraday cup was placed in the beam path at a distance of 10.25 inches from the skimmer orifice. Metastable argon atoms collide with a gold plated surface on the inside of the Faraday cup, ejecting electrons. The current produced is measured by an electrometer and is proportional to the metastable argon atom intensity.

The metastable beam intensity can be estimated from calculations using the following quantities: the secondary electron current, the secondary electron ejection coefficient and the beam dimensions. The secondary electron ejection coefficient for $Ar(^3P_{2,0})$ on a gold surface is 0.66 electrons/metastable atom.[69]

The electrometer signal was measured to be 0.975 V with a 10^9 ohm input resistor; therefore, the measured secondary electron current was 9.75×10^{-10} amp. The number of atoms detected per second is given by $(9.75 \times 10^{-10}$ amp$)(1.6 \times 10^{-19}$

Table 2

Metastable Beam Dimensions

A. Orifice diameters and slit dimensions (in.)	
Nozzle orifice	0.002
Skimmer orifice	0.040
Collimator orifice	0.079
Magnetic electron multiplier entrance slit (width)	0.010
Magnetic electron multiplier entrance slit (height)	0.250
B. Distances (in.)	
Nozzle to skimmer	0.42
Skimmer orifice to collimator	3.10
Collimator to chopper	0.10
Chopper to multiplier entrance slit	18.31

coulomb/electron)$^{-1}$(0.66 electron/atom)$^{-1}$ = 9.2 x 10^{9} atoms sec^{-1}. The solid angle subtended by the slit of the Faraday cup is calculated by dividing the slit area by the square of the skimmer-to-Faraday cup distance, i.e., (0.01 inch^2) (10.25 inch)$^{-2}$ = 9.5 x 10^{-5} steradians. Therefore, the metastable argon beam intensity is 9.7 x 10^{13} metastables steradian^{-1} sec^{-1}. This intensity is over 100 times greater than the value obtained by Sanders, 6 x 10^{11} metastables steradian^{-1} sec^{-1}, using an effusive type, D. C. discharge source with mechanical velocity selection in the same apparatus.[18]

In another series of preliminary experiments the velocity of ground state argon atoms was compared to the velocity of metastable argon atoms in the beam. The velocity of the ground state argon was measured with the quadrupole mass spectrometer, while the velocity of the metastable argon was measured with the magnetic electron multiplier. The velocity distributions of the two turned out to be significantly different, although both experiments were carried out under the same beam conditions and at the same temperature. The peak in the velocity distribution of ground state argon came at 576 meters sec^{-1}, and the peak of the metastable argon at 637 meters sec^{-1}, a faster value. No explanation of this difference is proposed at this time.

Under normal operation the glow discharge heats the metastable nozzle from its room temperature value. about 28°C with the diffusion pumps on, to a value of 43°C. This gives

a metastable argon velocity of 640 meters sec^{-1}. With the cooling system operating at full capacity under the same beam conditions the nozzle can be cooled to a value of -36°C which corresponds to a metastable argon velocity of 535 meters sec^{-1}. Therefore, by cooling the metastable argon velocity can be varied from 535 meters sec^{-1} to 640 meters sec^{-1}. The temperature, and thereby the velocity, is adjusted by changing the flow rate of cooled air through the nozzle jacket.

B. Target Beam

A characterization of the target beam has been conducted in detail previously by Sanders.[18] Since those studies were conducted, the only modification of the target nozzle has been the addition of a heater in the nozzle body. The heater is described in Chapter II D. Therefore, the only characterization studies described in this work have to do with the heating of the target beam.

The dimensions associated with the target beam are listed in Table 3.

Using the heater, the nozzle could easily be heated to 400°C. Equation (1) in Chapter II D predicts that the beam energy, and therefore the beam $(velocity)^2$, is directly proportional to the nozzle temperature. An experiment was conducted by measuring the N_2 beam energy as a function of temperature. The results are shown in Figure 14. The behavior is linear as predicted.

Table 3

Target Beam Dimensions

A. Orifice diameters and slit dimensions (in.)

Nozzle orifice	0.002
Skimmer orifice	0.040
Collimator orifice	0.079
Ionizer entrance slit (width)	0.070
Ionizer entrance slit (height)	0.250

B. Distances (in.)

Nozzle to skimmer	0.45
Skimmer orifice to collimator	2.80
Collimator to chopper	0.40
Chopper to ionizer slit	21.20

Figure 14. Temperature Dependence of N_2 Beam $(\text{Velocity})^2$

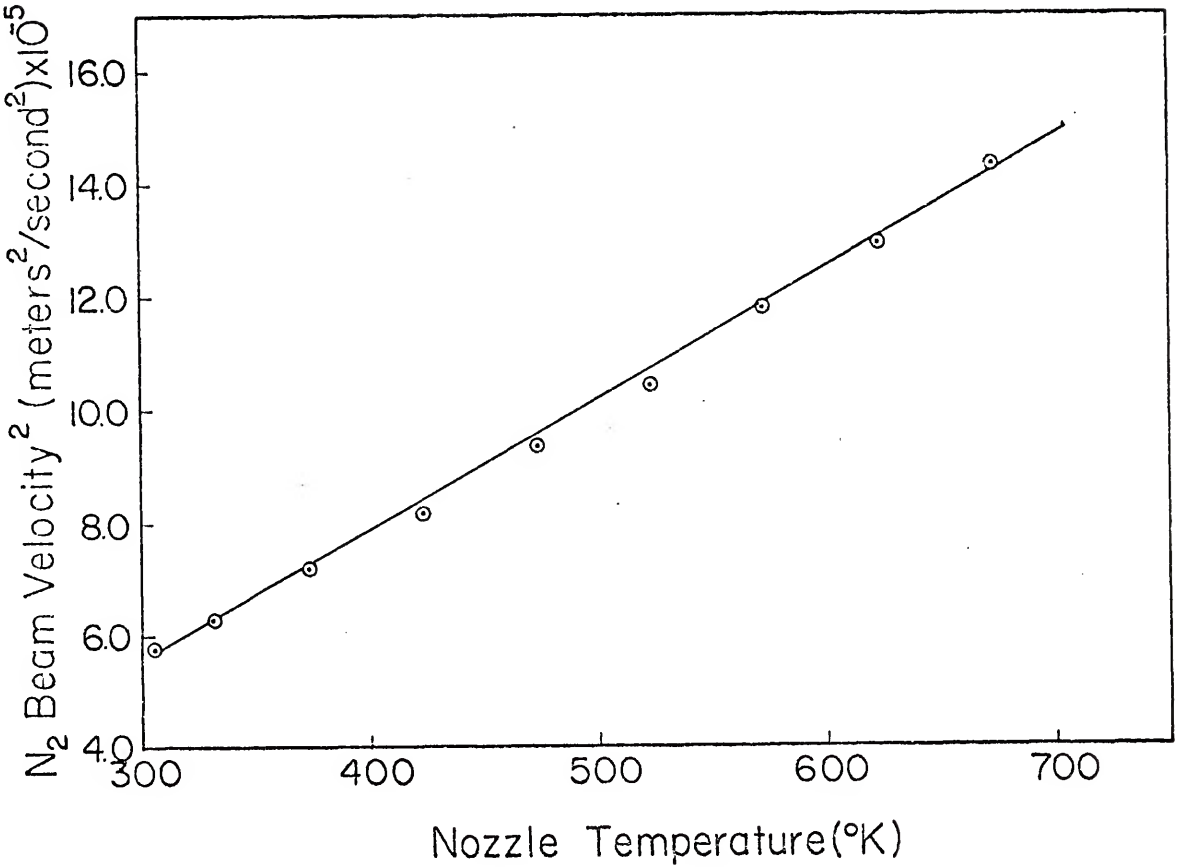
N_2 Beam Velocity^2 (meters^2/second^2)x10^{-5}
16.0
14.0
12.0
10.0
8.0
6.0
4.0
300
400
500
600
700
Nozzle Temperature(°K)

By a combination seeding and heating technique the range of the N_2 beam velocity could be varied from 579 meters sec^{-1} to 2095 meters sec^{-1}. The lowest velocity value for N_2 corresponds to "reverse" seeding the N_2 with argon at room temperature, and the highest velocity corresponds to seeding the N_2 with helium at 400°C.

CHAPTER V
DATA ANALYSIS AND RESULTS

A. Band Profile Measurements

Band profiles of the N_2 $C^3\Pi_u$ (v' = 0) to $B^3\Pi_g$ (v'' = 0) band, the (0 - 0) band, were measured at Ar* - N_2 relative energies of 0.074, 0.089 and 0.161 eV. These profiles are shown in Figures 15 through 17. Slits allowing a 10 Å bandpass were used in the monochromator for these measurements. The three measurements above were made with an unseeded N_2 beam. Higher relative energy measurements with seeded N_2 were not possible due to lack of intensity. Also, the N_2 $C^3\Pi_u$ (v' = 1) to $B^3\Pi_g$ (v'' = 0) band, the (1 - 0) band, was not intense enough for profile studies.

The emission intensities of the lines of a rotational-vibrational band, assuming a thermal distribution of rotational levels, is given by the following:[70]

$$I_{em} = \frac{2\, C_{em} \nu^4}{Q_r} S_J \exp\,[-B_{v'} J'(J' + 1)hc/kT] \qquad (4)$$

where C_{em} is a constant depending on the change of dipole moment and the total number of molecules in the initial vibrational level, Q_r is the rotational partition function, ν is the frequency of the emitted light, J' is a rotational level

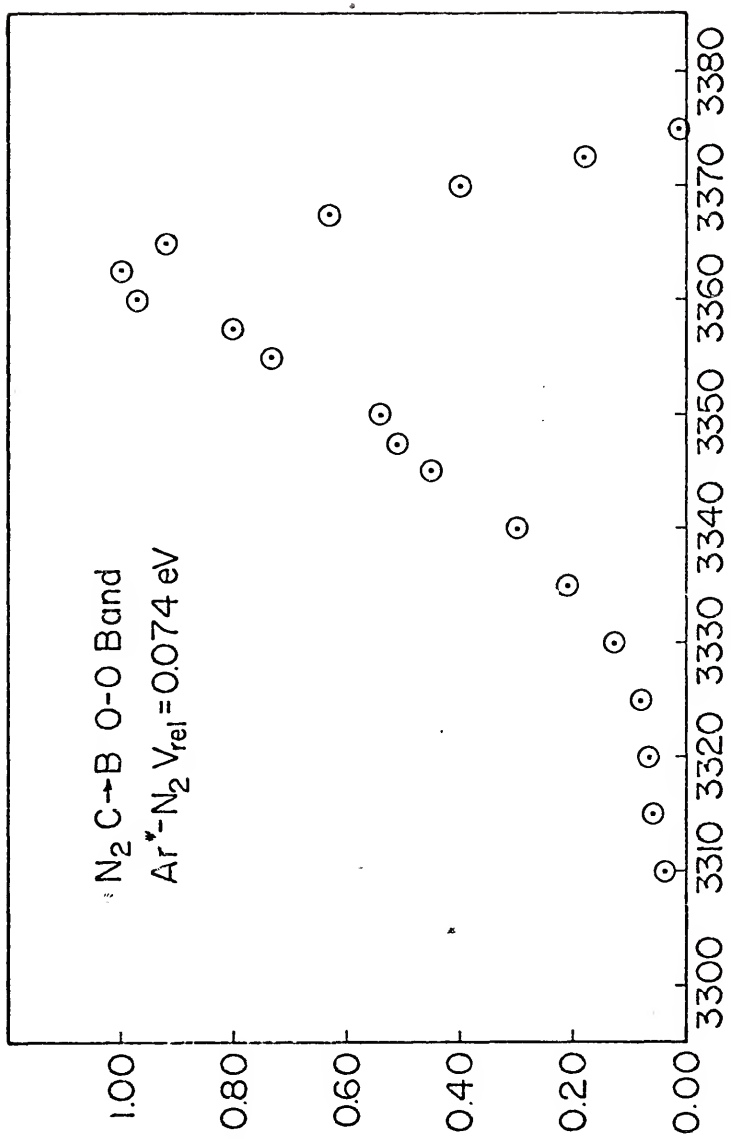

Figure 15. N_2 (0 - 0) Band Profile, 0.074 eV

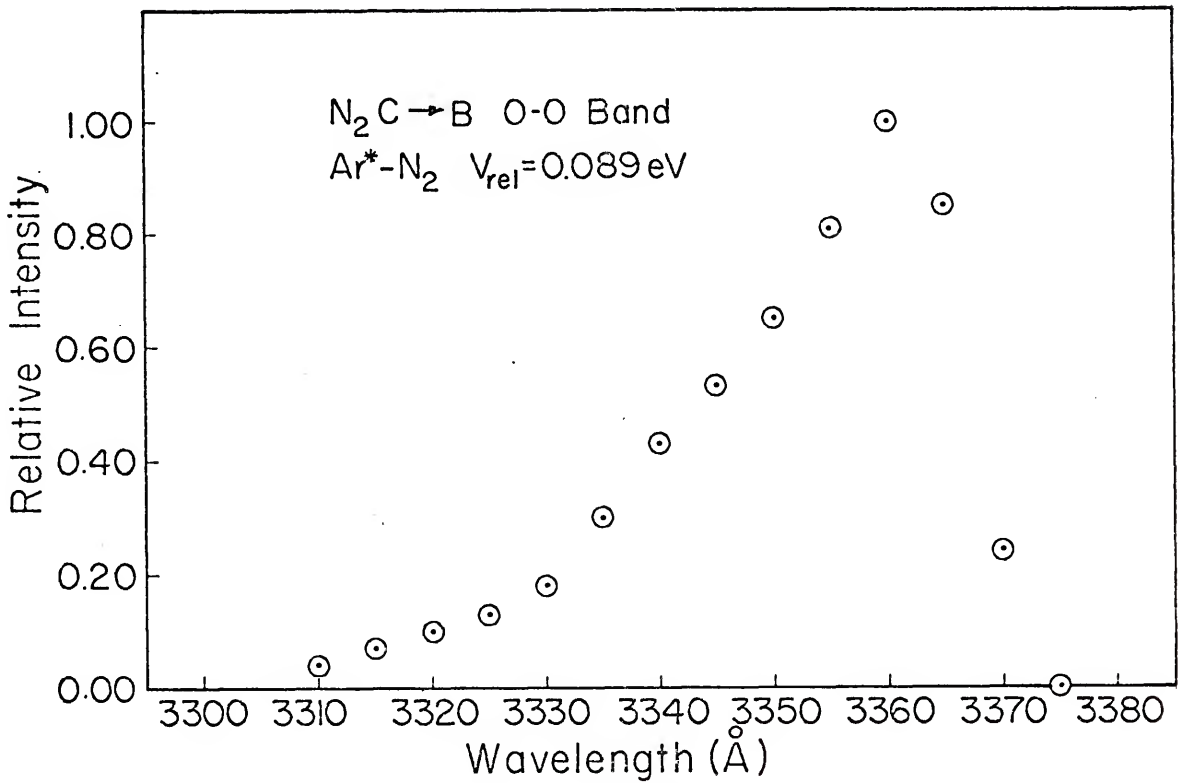

Figure 16. N_2 (0 - 0) Band Profile, 0.089 eV

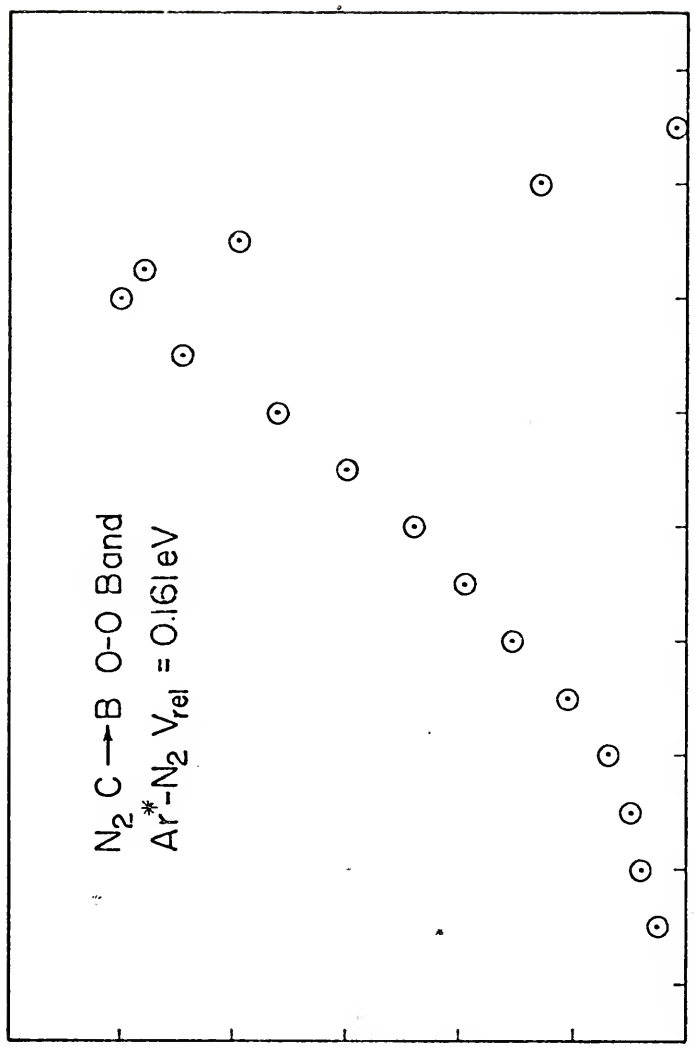

Figure 17. N_2 (0 - 0) Band Profile, 0.161 eV

in the upper state, $B_{v'}$ is the rotational constant of the upper state vibrational level, S_J is the "line strength," and the remaining variables have their standard meaning.

The "line strengths" of a symmetric top molecule have been derived by Honl and London.[71] For the R branch of a rotational - vibrational band in an electronic transition with $\Delta\Lambda = 0$, S_J is given by the following:

$$S_J^R = \frac{(J' + \Lambda')(J' - \Lambda')}{J'} \qquad (5)$$

In the case under consideration here, a $C^3\Pi_u \rightarrow B^3\Pi_g$ transition, $\Lambda' = 1$. Therefore, S_J^R is given by the following:

$$S_J^R = \frac{(J' - 1)^2}{J'} \qquad (6)$$

Equation (4) can be transformed into the equivalent form:

$$\ln\left(\frac{I_{em}}{S_J}\right) = A - \frac{B_{v'}J'(J' + 1)hc}{kT} \qquad (7)$$

where $A = \ln (2\, C_{em}\nu^4/Q_r)$ may be considered a constant since for a given band ν covers only a very small range of values. Again, assuming a thermal distribution of rotational levels, a plot of $\ln (I_{em}/S_J)$ against $J'(J' + 1)$ should give a straight line of slope $-B_{v'}hc/kT$. Therefore, the "rotational" temperature of the transition can be calculated.

The above calculation was carried out for the three line profiles measured in this work, and plots of $\ln (I_{em}/S_J)$ vs. $J'(J' + 1)$ are shown in Figures 18 through 20. A least squares procedure was used to calculate the slope. Rotational temperatures of 1090 and 1280°K were calculated for the relative

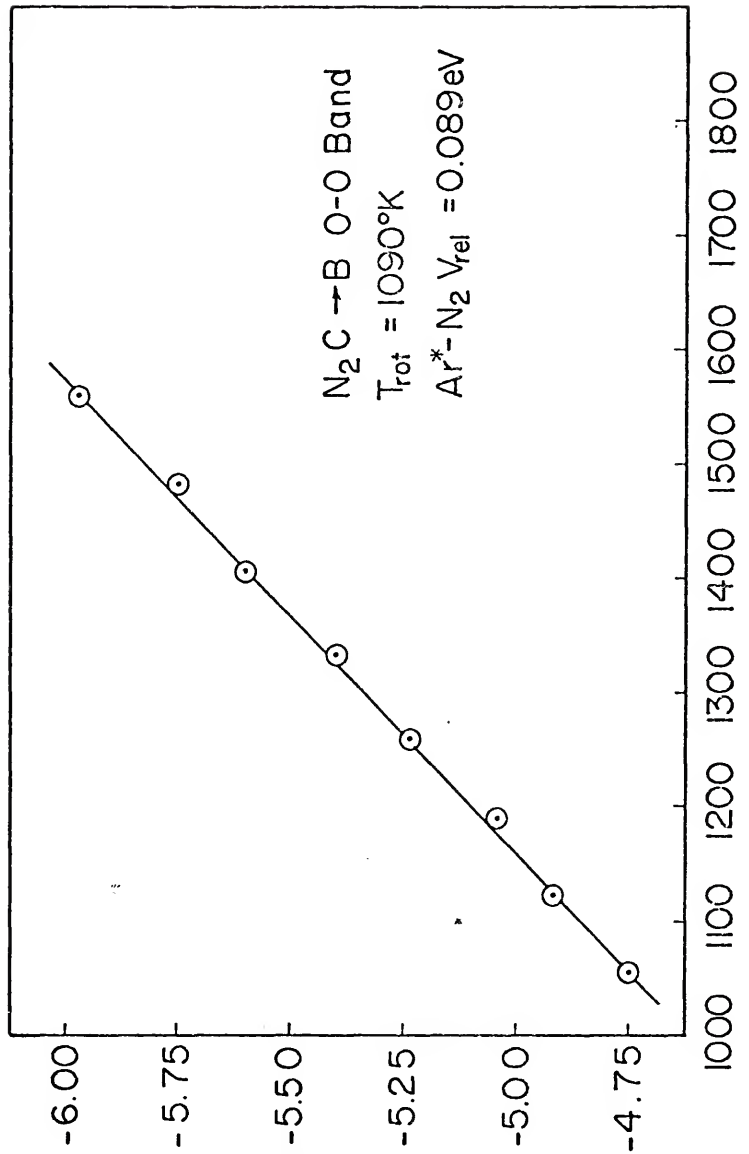

Figure 18. Rotational Temperature Plot, 0.089 eV

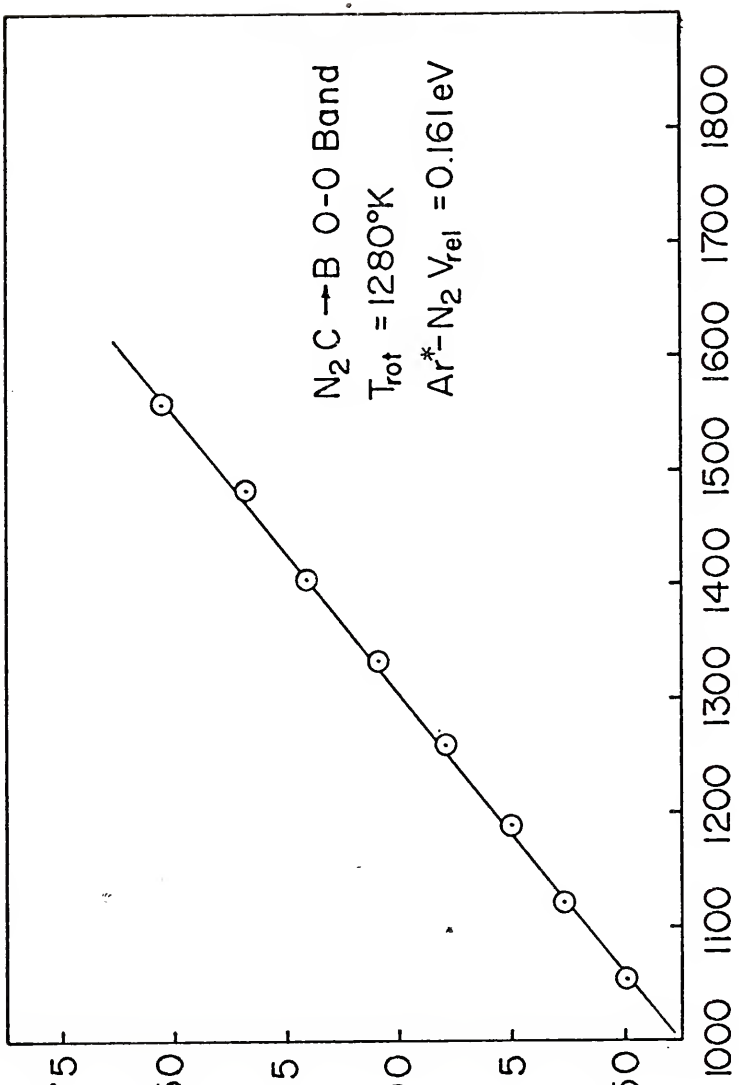

Figure 19. Rotational Temperature Plot, 0.161 eV

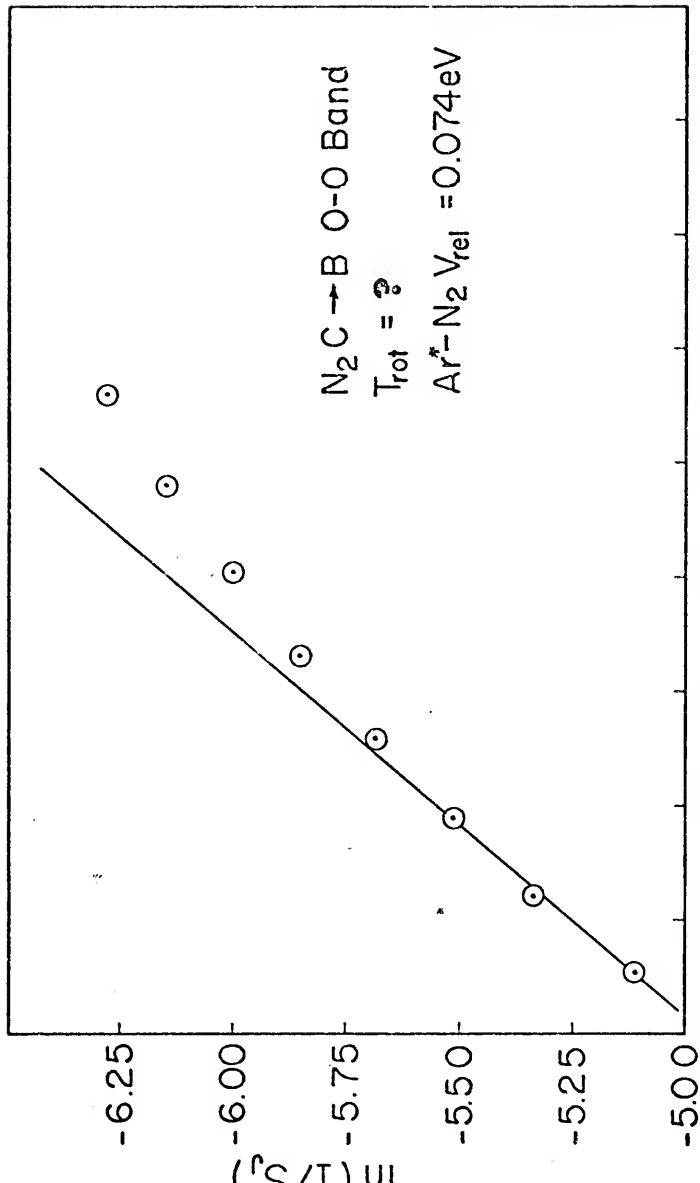

Figure 20. Rotational Temperature Plot, 0.074 eV

energies of 0.089 and 0.161 eV, respectively. At 0.074 eV the plot was not linear, and therefore a rotational temperature could not be calculated.

For these calculations the wavelength of rotational-vibrational transitions of a particular J value in the R branch were determined from high resolution work done on this transition by Setser et al.[72] Relative intensities at these wavelengths were then determined using the low resolution band profiles, and these values were substituted into equation (7) for I_{em}.

B. Branching Ratio Measurements

Data were collected for the (0 - 0) and (1 - 0) bands as described in Chapter III. The signal-averaged photon count rates were recorded once every 100 sec of counting time. Typical photon count rates for the (0 - 0) and (1 - 0) bands were about 1000 and 250 counts sec^{-1}, respectively. These values were somewhat smaller at the higher relative energies where a large amount of seeding gas had to be used in the target gas flow. Measurements were made in the energy range 0.053 - 0.408 eV.

For a particular relative energy the average photon count rate for each band was calculated by a minicomputer.[73] A special program was written for the minicomputer for this purpose. In this program the mean count rate and the standard deviation of the mean (S. D./$\sqrt{n}$, where S. D. is the standard

deviation of the data and n is the number of data) are calculated. The minicomputer rejects any data greater or less than two standard deviations of the mean from the mean and recalculates the mean count rate. The mean count rate for each band is then divided by its appropriate Franck-Condon factor to give a photon count rate which is proportional to the vibrational population of either the v' = 1 or v' = 0 level of the N_2 C state.[74] For example, the (0 - 0) band count rate is divided by the v' = 0 to v'' = 0 Franck-Condon factor (0.4527) to give a number which would be the photon count rate for all transitions from the zeroth vibrational level of the C state to any vibrational level in the B state, i.e., a number proportional to the population of the zeroth vibrational level of the C state. For the (1 - 0) band a Franck-Condon factor of 0.3949 was used. Calculation of the branching ratio (v' = 0)/(v' = 1) follows directly from the two Franck-Condon corrected photon count rates. The experimental results obtained are shown in Figure 22 (Chapter VI B).

It should be mentioned that the error bars on these points are no larger than the circles drawn around each point. This is due to the fact that the photon count rates were 3 - 4 times as great as the background count rates in each measurement.

CHAPTER VI
DISCUSSION

A. Band Profile Measurements

A comparison of the low wavelength tail of the three band profiles is shown in Figure 21. All three profiles are normalized to their peak height. As is expected, the higher relative translational energy measurements show more rotational excitation at the higher J values. The rotational temperatures calculated and their respective relative translational energies are the following: 0.089 eV - 1080°K and 0.161 eV - 1280°K.

If a thermal distribution of rotational levels were present in all three measurements, the plots of ln (I/S_J) vs. $J(J + 1)$ should all be linear. Looking at the plots of ln (I/S_J) for the three profiles in Figures 18 through 20, it can be seen that the plots for relative translational energies of 0.089 and 0.161 eV are linear, and a thermal distribution of rotational levels exists. However, the plot at 0.074 eV is not linear; therefore, the rotational levels are not distributed thermally. This may be due to the fact that the threshold energy for the reaction $Ar^* + N_2(X) \rightarrow Ar + N_2(C)$ is approximately 0.05 eV as measured by Sanders.[18] Further supportive evidence for this threshold was found in this work. At the

Figure 21. Comparison of the Low Wavelength Tail of the Band Profiles

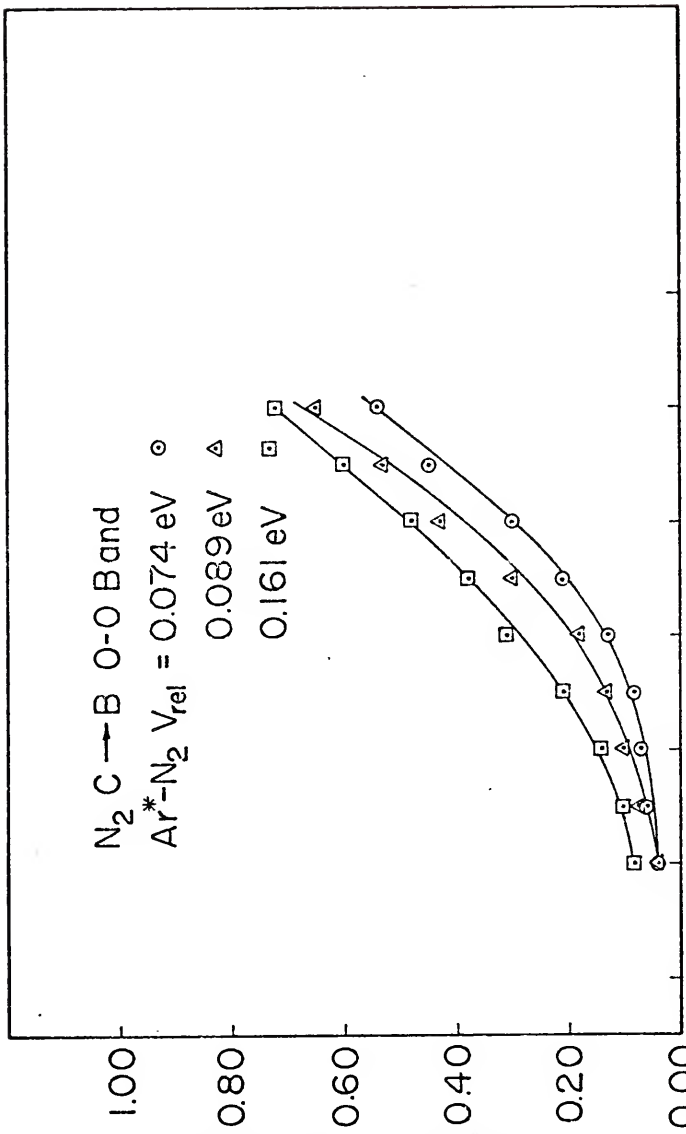
N_2 C → B 0-0 Band
Ar^*-N_2 V_{rel} = 0.074 eV
0.089 eV
0.161 eV
Relative Intensity
1.00
0.80
0.60
0.40
0.20
0.00
3300 3310 3320 3330 3340 3350 3360
Wavelength (Å)

lower relative energy branching ratio measurements a gradual decrease in photon intensity was observed. The lowest relative energy line profile (0.074 eV) could be near enough to the threshold that the rotational distribution of levels is affected in some way.

B. Branching Ratio Measurements

A reaction dynamics model which predicts product vibronic state distributions in collision-induced electronic-to-vibrational energy transfer processes has been proposed by Berry.[75] In this model the interaction which leads to electronic energy transfer is treated by perturbation theory.[76,77] For a perturbation V which is independent of time the relative transition probabilities $W_{i\to f}$ for formation of final product states can be calculated directly by a first order treatment of the Fermi Golden Rule:[75]

$$W_{i\to f} = (2\pi/\hbar)|\langle f|V|i\rangle|^2 \rho_f(\varepsilon) \qquad (8)$$

where $\rho_f(\varepsilon)$ is the density-of-final-states function and ε is the mean available energy for the vibrational state in question. In these studies i refers to the zeroth vibrational level of the N_2 X state, and f refers to either the zeroth or first vibrational level in the N_2 C state. Assuming the energy transfer from metastable argon to the N_2 molecule occurs very suddenly, the matrix elements in equation (8) become Franck-Condon factors for the initial and final oscillator states:[75]

$$|\langle f|V|i\rangle|^2 \quad \alpha \quad |\langle f|i\rangle|^2 \tag{9}$$

The density-of-final-states function $\rho_f(\varepsilon)$ used by Berry assumes a vibrating rotator model for N_2 and was derived by Ben-Shaul et al. for the atom + diatom case to be the following:

$$\rho_f(\varepsilon) \quad \alpha \quad (1 - f_{v'})^{3/2} \; / \; \sum_{v'}(1 - f_{v'})^{3/2} \tag{10}$$

where $f_{v'}$ is the fraction of mean available energy ε channeled into vibration in a particular product vibrational state v'.[75,78]

The present study is only concerned with the N_2 C state population ratio $(v' = 0)/(v' = 1)$. This ratio can be calculated from the ratio of the relative transition probabilities:

$$\frac{W_o}{W_1} = \frac{|\langle 0_c|0_x\rangle|^2}{|\langle 1_c|0_x\rangle|^2} \frac{\rho_o(\varepsilon)}{\rho_1(\varepsilon)} \tag{11}$$

Since f_o in $\rho_o(\varepsilon)$ is zero, the above expression reduces to the following:

$$\frac{W_o}{W_1} = 1.792 \; (1 - f_1)^{-3/2} \tag{12}$$

where the Franck-Condon factors used are those calculated by Benesch et al. and f_1 is the fraction of mean available energy going into vibrational state 1.[79] f_1 is calculated from the following:

$$f_1 = \frac{E(C,v' = 1) - E(C,v' = 0)}{\text{R.K.E.} + \bar{E}_{Ar^*} - E(X,v'' = 0 \rightarrow C,v' = 0)} \tag{13}$$

where R.K.E. represents the relative kinetic energy of the

Ar* - N_2 and the electronic and vibrational spacings were obtained from Benesch et al.[80] The statistical average metastable energy $\bar{E}_{Ar^*}$ was calculated from $^3P_{2,0}$ energy values given by Setser et al. assuming both metastable components are equally reactive and present in a statistical distribution.[72]

The transition probability ratio W_o/W_1 was calculated over the R.K.E. range 0 - 0.40 eV and is plotted against R.K.E. along with the experimentally determined branching ratio in Figure 22. The Golden Rule model fits the data reasonably well at the lower energy values; however, the fit is poor at the higher energy values. Also, the two curves do not have the same shape. The curves suggest that the standard Franck-Condon controlled excitation process from the N_2 X state to the N_2 C state does not play a major role in the energy transfer at the higher energy values. These findings agree with the work of Stedman and Setser concerning the dynamics of reactions of metastable rare gas atoms.[81] Their generalization that "neutral excitation is not expected to follow Franck-Condon excitation" is correct for the Ar* - N_2 system at the higher relative energy values.[81]

As a qualitative explanation of the branching ratio vs. R.K.E. curve, consider the following model. During the Ar* - N_2 collision the wavefunction of the N_2 X state is perturbed. The perturbed wavefunction describes an N_2 molecule with a weakened N - N bond; the amount of weakening depending on the turning point in the collision and hence on the R.K.E. Therefore, the higher the R.K.E. the larger r_e is for the perturbed wavefunction.

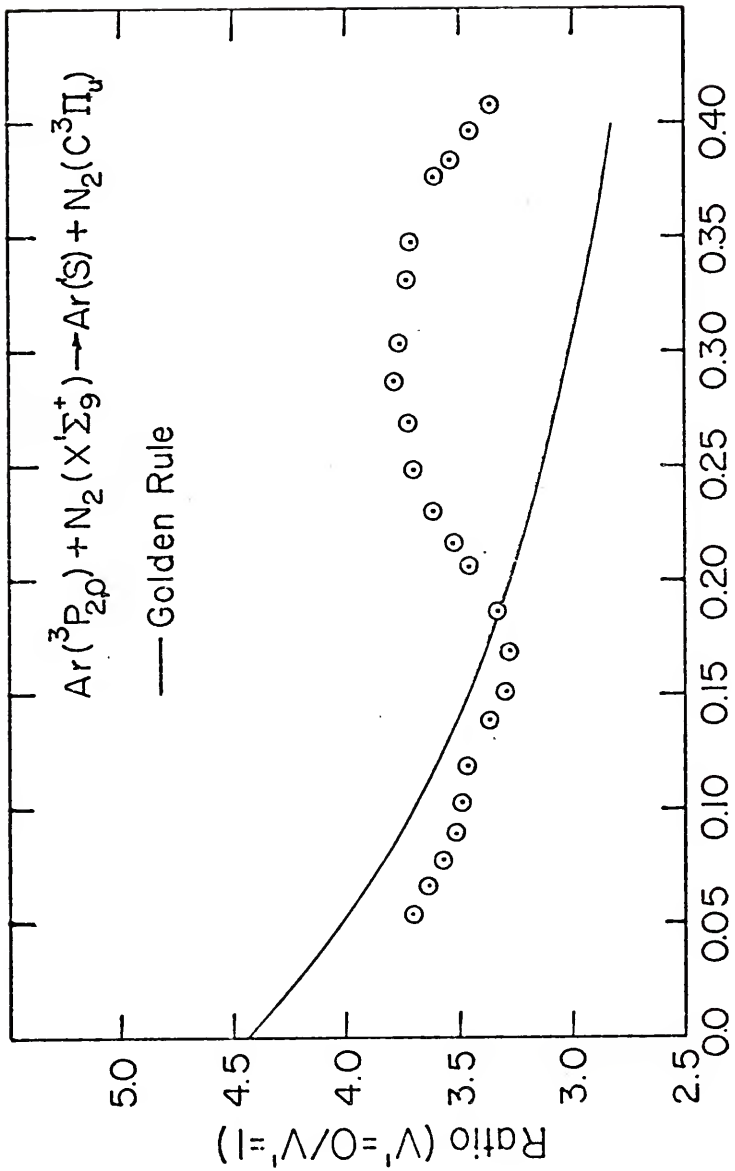

Figure 22. N_2 C State Population Ratio (v' = 0)/(v' = 1)

Now consider the energy level diagrams given in Figure 23. The shape of the harmonic oscillator wave functions for the zeroth vibrational level of the X state and the zeroth and first vibrational levels of the C state are shown. The minima of both electronic states are shown at their standard r_e values, and both are referenced to zero potential energy. In the above proposed model the r_e value is assumed to increase with increasing R.K.E. As r_e starts to increase the overlap, and therefore the transition probability, between the C state first vibrational level wave function and the X state zeroth vibrational level wave function, the (1 - 0) overlap, reaches its maximum value, while the (0 - 0) overlap is still slowly increasing. Therefore, the branching ratio would decrease at first. As r_e increases further, the (0 - 0) overlap reaches its maximum value, and the (1 - 0) overlap its minimum value causing the branching ratio to increase. And finally, the (0 - 0) overlap begins decreasing again, and the (1 - 0) overlap begins increasing to its maximum value again causing the branching ratio to go back down. Although this is only a qualitative explanation for the change in the branching ratio, it does seem to explain the general shape of the curve.

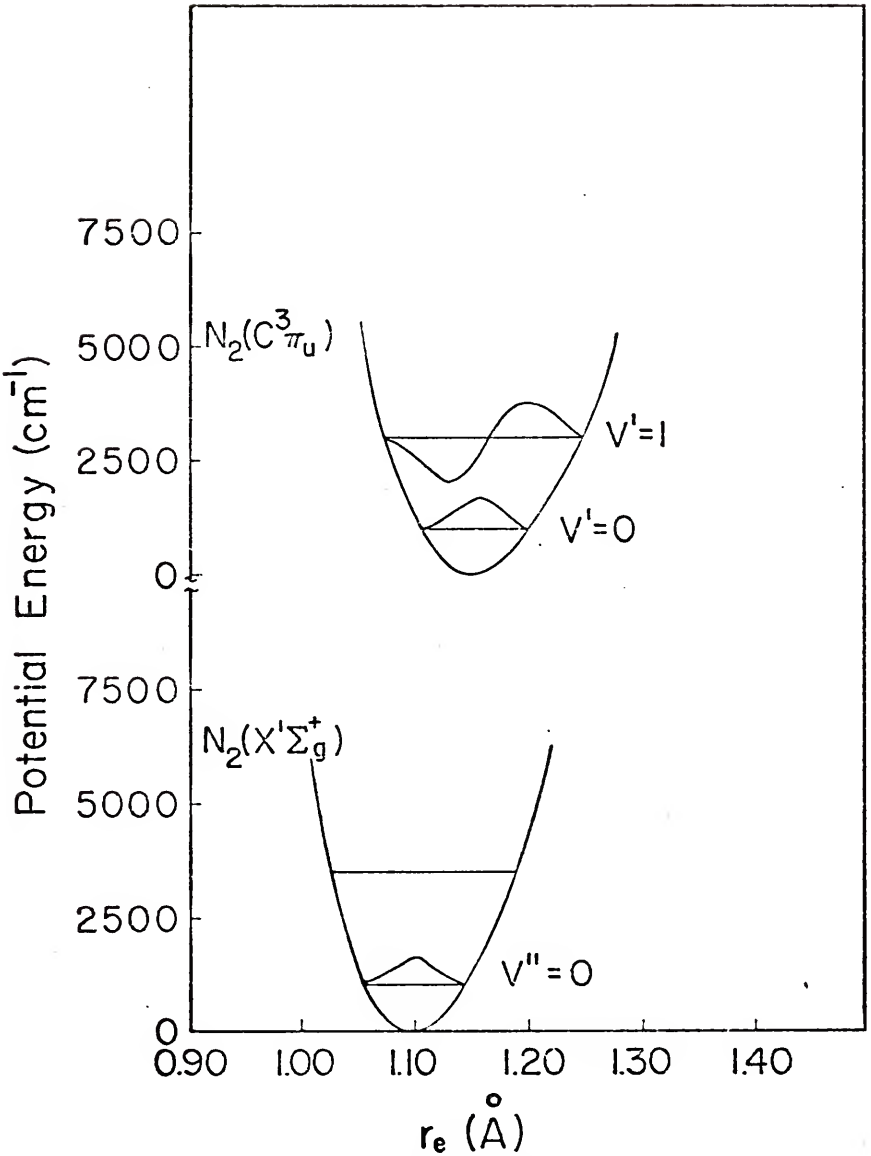

Figure 23. N_2 Potential Energy Diagram

REFERENCES

1. J. A. Fleming, The Electrician, 11, 65, 1883.

2. L. Dunoyer, Le Radium, 8, 142, 1911.

3. W. Gerlach and D. Stern, Z. Physik, 8, 110, 1921.

4. T. H. Johnson, J. Franklin Inst., 206, 301, 1928.

5. A. Kantrowitz and J. Grey, Rev. Sci. Instr., 22, 328, 1951.

6. G. B. Kistiakowsky and W. P. Slichter, Rev. Sci. Instr., 22, 333, 1951.

7. E. W. Becker and K. Bier, Z. Naturforsch., 9A, 975, 1954.

8. E. W. Becker and W. Henkes, Z. Physik, 146, 320, 1956.

9. A. N. Schweid, M. A. D. Fluendy and E. E. Muschlitz, Jr., Chem. Phys. Lett., 42, 103, 1976.

10. C. K. N. Patel, "Lasers," Vol. 2, A. K. Levine, ed., E. Arnold and Co., London, 1968.

11. Michael E. Gersh and E. E. Muschlitz, Jr., J. Chem. Phys., 59, 3538, 1973.

12. Wellington Lee and Richard M. Martin, J. Chem. Phys., 64, 678, 1976.

13. R. A. Sanders, A. N. Schweid, M. Weiss and E. E. Muschlitz, Jr., J. Chem. Phys., 65, 2700, 1976.

14. D. W. Martin, T. Fukuyama, R. W. Gregor, R. M. Jordan and P. E. Siska, J. Chem. Phys., 65, 3720, 1976.

15. K. J. Laidler, "The Chemical Kinetics of Excited States," Oxford University Press, Amen House, London, 1955, p. 87.

16. E. S. Fishburne, J. Chem. Phys., 47, 58, 1967.

17. E. Fink and K. H. Welge, Z. Naturforsch., 19A, 1193, 1964.

18. R. A. Sanders, Ph. D. Dissertation, University of Florida (1975).

19. Cenco, Hyvac 2, Central Scientific Co., Chicago, IL, Serial Number 1506.

20. Speedivac, Edwards High Vacuum, Ltd., Manor Royal, Crawley, Sussex. Model 8-1, range 10^{-3} - 10 torr.

21. Aktomatic Valve Co., Inc., Indianapolis, Ind., Model TT 204.

22. Vactonic Lab Equipment Inc., East Northrop, N. Y., Model VVB-50-S.

23. Wallace and Tiernan Division, Penwalt Corporation, Belleville, N. J., Model FA 160, range 0 - 30 PSIA.

24. Nupro Company, Cleveland, Ohio, Model B-2FR-7.

25. The Welch Scientific Company, "Duo Seal" Vacuum Pump, Model 1400.

26. Consolidated Vacuum Corporation, Rochester, N. Y.
    (a) Model GTC-100
    (b) Model B, 10"; maximum pumping speed in air 2500 l/sec.

27. Teledyne-Hastings-Raydist, Hampton, VA.
    For helium and argon Model ALL-100P, range 0 - 100 SCCM.
    For nitrogen Model ALL-50P, range 0 - 50 SCCM.

28. NRC Operation, Varian Vacuum Division, Newton, Mass.
    (a) Model VHS-6; maximum pumping speed for air 2400 l/sec.
    (b) Model 336.

29. General Radio, West Concord, Mass., Model W30H.

30. Bendix Scientific Instruments and Equipment, Rochester, N. Y., Model BC-016.

31. Sargent-Welch Scientific Company, Skokie, IL, Welch "Duo Seal" Vacuum Pumps.
    Target gas chamber: Model 1375.
    Metastable chamber and main chamber: Model 1397.

32. Main chamber: Veeco Instruments Company, Plainview, N. Y., Model TC-9.
    Metastable and target gas chambers: NRC, Newton, Mass., Model 836.

33. Veeco Instruments Company, Plainview, N. Y., Model RG75K.

34. Pelco Electron Microscopy Supplies, Ted Pella Company, Tustin, CA, Model 603-C.

35. Omega Engineering, Inc., Stamford, Conn.
    (a) Model 50J.
    (b) Model 50K.

36. Trygon Electronics, Inc., Roosevelt, N. Y., Model M36-30A.

37. Lambda Electronics Corporation, Huntington, N. Y., Model LP-524-FM.

38. Sorenson Power Supplies, Raytheon Company, Manchester, N. H., Model DCR150-2.5A.

39. Bendix Corporation, Cincinnati Division, Cincinnati, Ohio, Model 306.

40. Keithley Instruments, Inc., Cleveland, Ohio, Model 603.

41. United Systems Corporation, Dayton, Ohio, Model 266.

42. Leeds and Northrup, Philadelphia, PA, Speedomax G.

43. J. P. Tonnies, in W. Jost, ed., "Physical Chemistry, An Advanced Treatise," VIA, 227, Academic Press, New York, N. Y., 1974.

44. Peter P. Wegener, ed., "Molecular Beams and Low Density Gasdynamics," Marcel Dekker, Inc., New York, 1974.

45. J. B. Anderson and J. B. Fenn, Phys. Fluids, 8, 780, 1965.

46. Globe Industries of TRW, Inc., Dayton, Ohio, Model 53A118-2.

47. Krohn-Hite Corporation, Cambridge, Mass. Models 440A(R) and DCA-10(R).

48. Electronic Associates, Inc., Palo Alto, Calif.
(a) Quadrupole Model 210.
(b) 14 stage with Cu-Be dynodes.

49. See reference 1, Appendix 1.

50. See reference 1, Appendix 2.

51. See reference 1, Appendix 3.

52. Princeton Applied Research, Princeton, N. J.
(a) Model 121 lock-in amplifier.
(b) Model TDH-8 waveform eductor.

53. United Systems, Inc., Cleveland, Ohio, Model 603.

54. Hewlett-Packard Company, Palo Alto, Calif.
(a) Model 140A dual beam oscilloscope.
(b) Model 214A pulse generator.

55. Elscint Ltd., Haifa, Israel, Model CRC-N-1.

56. Rolyn Optics Company, Arcadia, Calif.
(a) Stock number 61.2200, radius of curvature 20.0 mm.
(b) Stock number 11.2050, focal length 25.0 mm.
(c) Stock number 11.2650, focal length 200.0 mm.
(d) Stock number 11.2300, focal length 100.0 mm.

57. Spex Industries, Inc., Metuchen, N. J., Spex Minimate Model 1670.

58. EMI, Gencom Division, Plainview, N. Y., Model 9558, with an extended red response S-20 cathode.

59. Products for Research, Inc., Danvers, Mass., Model TE-104TS-RF.

60. Northeast Scientific Company, Acton, Mass., Model RE-5006, 5 kV.

61. SSR Instruments Company, Santa Monica, Calif.
(a) Model 1120 amplifier/discriminator
(b) Model 1110 digital synchronous computer.

62. United Systems Corporation, Dayton, Ohio.
(a) Digitec Model 266 DVM.
(b) Datos Model 305 Data Coupler.

63. Newport Laboratories, Inc., Santa Ana, Calif., Model 200A/S.

64. Teletype Corporation, Skokie, Ill., Model 33TC.

65. G. Bertschinger, H. Schmid and H. v. Buttlar, Z. Physik, 268, 129, 1974.

66. John's Technology, Inc., Livermore, Calif., Model T-11.

67. Weston Electrical Instruments Company, Newark, N. J., Model 931.

68. William Benesch and Joseph T. Vanderslice, Ap. J., 143, 408, 1965.

69. F. B. Dunning and A. C. H. Smith, J. Phys. B: Atom. Molec. Phys., 4, 1696, 1971.

70. Gerhard Herzberg, "Spectra of Diatomic Molecules," 2nd Ed., D. Van Nostrand Company, Inc., Princeton, N. J., 1950, p. 126.

71. H. Honl and F. London, Z. Physik, 33, 803, 1925.

72. D. W. Setser, D. H. Stedman and J. A. Coxon, J. Chem. Phys., 53, 1004, 1970.

73. Digital Computer Controls, Inc., Fairfield, N. J., Model D-416.

74. W. Benesch, J. T. Vanderslice, S. G. Tilford and P. G. Wilkinson, Ap. J., 144, 408, 1966.

75. Michael J. Berry, Chem. Phys. Lett., 29, 329, 1974.

76. J. Jortner, S. A. Rice and R. M. Hochstrasser, Advan. Photochem., 7, 148, 1969.

77. M. L. Goldberger and K. M. Watson, "Collision Theory," John Wiley and Sons, Inc., New York, N. Y., 1964, Ch. 8.

78. A. Ben-Shaul, R. D. Levine and R. B. Bernstein, J. Chem. Phys., 57, 5427, 1972.

79. W. Benesch, J. T. Vanderslice, S. G. Tilford and P. G. Wilkinson, Ap. J., 143, 236, 1966.

80. W. Benesch, J. T. Vanderslice, S. G. Tilford and P. G. Wilkinson, Ap. J., 142, 1227, 1965.

81. D. H. Stedman and D. W. Setser, "Progress In Reaction Kinetics, Vol. 6," 1971, p. 193.

BIOGRAPHICAL SKETCH

Euel Ray Cutshall was born March 31, 1950, in Sheffield, Alabama. He graduated from Coffee High School in Florence, Alabama, in 1967. He entered the University of North Alabama in 1967 and graduated with a Bachelor of Arts degree in both Chemistry and Mathematics in 1972. After serving a three month tour of duty for training purposes in the U. S. Army, he entered the Graduate School at the University of Florida. From 1973 to present he has pursued studies in Chemistry leading to the degree of Doctor of Philosophy.

He is married to the former Linda Washburn, who received her Bachelor of Arts degree in Early Childhood Education from the University of Florida in 1976, and has a young son, Christopher.

I certify that I have read this study and that in my opinion it conforms to acceptable standards of scholarly presentation and is fully adequate, in scope and quality, as a dissertation for the degree of Doctor of Philosophy.

E. E. Muschlitz, Jr.
E. E. Muschlitz, Jr., Chairman
Professor of Chemistry

I certify that I have read this study and that in my opinion it conforms to acceptable standards of scholarly presentation and is fully adequate, in scope and quality, as a dissertation for the degree of Doctor of Philosophy.

Charles P. Luehr
Charles P. Luehr
Associate Professor of Mathematics

I certify that I have read this study and that in my opinion it conforms to acceptable standards of scholarly presentation and is fully adequate, in scope and quality, as a dissertation for the degree of Doctor of Philosophy.

Willis B. Person
Willis B. Person
Professor of Chemistry

I certify that I have read this study and that in my opinion it conforms to acceptable standards of scholarly presentation and is fully adequate, in scope and quality, as a dissertation for the degree of Doctor of Philosophy.

Thomas L. Bailey
Professor of Physics

I certify that I have read this study and that in my opinion it conforms to acceptable standards of scholarly presentation and is fully adequate, in scope and quality, as a dissertation for the degree of Doctor of Philosophy.

Samuel O. Colgate
Associate Professor of Chemistry

This dissertation was submitted to the Graduate Faculty of the Department of Chemistry in the College of Arts and Sciences and to the Graduate Council, and was accepted as partial fulfillment of the requirements for the degree of Doctor of Philosophy.

June 1977

Dean, Graduate School